

2012

High Throughput Evaluation of the Influence of Inorganic Salt Solutions on Nonionic

Eric R. Theiner
Lehigh University

Follow this and additional works at: <http://preserve.lehigh.edu/etd>

Recommended Citation

Theiner, Eric R., "High Throughput Evaluation of the Influence of Inorganic Salt Solutions on Nonionic" (2012). *Theses and Dissertations*. Paper 1069.

This Thesis is brought to you for free and open access by Lehigh Preserve. It has been accepted for inclusion in Theses and Dissertations by an authorized administrator of Lehigh Preserve. For more information, please contact preserve@lehigh.edu.

High Throughput Evaluation of the Influence of Inorganic Salt Solutions on Nonionic
Surfactant Aggregation Properties

by

Eric R. Theiner

A Thesis

Presented to the Graduate and Research Committee

of Lehigh University

in Candidacy for the Degree of

Master of Sciences

in

Chemistry

Lehigh University

April 17, 2012

© 2012 Copyright
Eric R. Theiner

Thesis is accepted and approved in partial fulfillment of the requirements for the Master of Science in Chemistry.

High Throughput Evaluation of the Influence of Inorganic Salt Solutions on Nonionic Surfactant Aggregation Properties
Eric R. Theiner

Date Approved

Dr. Tianbo Liu

Dr. Rebecca S. Miller

Dr. Robert A. Flowers

DEDICATION

To Sharon, for her indefatigable support and understanding, and to Charles and Thomas, for their willingness to let their dad periodically disappear for days at a time. Seeing my love of learning reflected in them is more rewarding than any degree could be.

ACKNOWLEDGMENTS

Although I had never intended to return to school, the past few years have been rewarding beyond anything I ever imagined. I would be remiss to not acknowledge the direct and indirect support that I received from my supervisors and coworkers at Air Products over the past few years, particularly David K. Moss, Richard J. Goddard, and Amir Famili. There are two men in particular who probably never realized the influence they had on my decision to seek an advanced degree, Robert E. Stevens and Scott Hanton. I owe all of them and many un-named colleagues a great deal.

Regarding actual aid, I gratefully acknowledge Renae J. Bennett and Debashis Neogi for their time spent helping me to learn to work with much of the equipment, systems, and software that were vital to this study; Renae in the lab and Debashis on the computer.

Lastly, I must thank James E. Roberts for convincing me to take his Chemometrics course, through which a nexus formed from my interest in modern technology, surface chemistry, and exploring unknown issues. The subject of this paper has interested me for quite some time, but it is only because of his class that I learned to use the tools needed to pursue it.

TABLE OF CONTENTS

LIST OF FIGURES.....	vii
LIST OF CHARTS.....	viii
LIST OF TABLES.....	x
ABSTRACT.....	1
CHAPTER	
1 INTRODUCTION	2
2 THEORETICAL FRAMEWORK.....	5
2.1 Importance of Micellar Relaxation Time.....	5
2.2 Describing Migration to an Interface.....	7
2.3 Micellar Impact Upon Adsorption.....	9
3 MATERIALS AND METHODS.....	11
3.1 Chemicals.....	11
3.2 High Throughput Sample Preparation.....	13
3.3 Instrumentation.....	13
4 EXPERIMENTAL PROCESS AND RESULTS.....	15
4.1 Critical Micelle Concentration.....	15
4.2 Surface Excess Concentration.....	23
4.3 Free Energies.....	24
4.4 Diffusion to a New Interface.....	26
4.5 Adsorption at the Interface.....	30
4.6 Rate of Demicellization.....	33
5 DISCUSSION OF RESULTS.....	37
6 CONCLUSION.....	43
REFERENCES.....	45
APPENDICES	
A: STANDARDIZING THE JANUS FORMULATOR.....	48
B: PHOTOMETRIC METHOD TO ELIMINATE OUTLIERS.....	64
VITA.....	79

LIST OF FIGURES

1. Illustration of Surfactant States at Solution Equilibrium.....	6
2. Maximal Micelle Stability for Sodium Dodecylsulfonate Juxtaposed with Performance Properties	6
3. Illustration of a Maximum Bubble Pressure Dynamic Tensiometer.....	26

LIST OF CHARTS

1.	Relative Percentages of Ethylene Oxide Adducts for.....	3
	Industrially Produced 2-Ethylhexanol Ethoxylates	
2.	Relative Distribution of Ethoxomers Present in the.....	11
	Nonionic Surfactant (C9-7EO) Studied	
3.	Equilibrium Surface Tension as a Function of C9-7EO.....	16
	Concentration in Water	
4.	Prediction Plot for Pre-Micellar C9-7EO Aqueous.....	18
	Concentration Regressed Model (All Data Retained)	
5.	Residuals Plot for Pre-Micellar C9-7EO Aqueous.....	19
	Concentration Regressed Model (Accepted Model)	
6.	Examination of Potentially Erroneous Points Identified from Chart 3...	20
7.	Normal Plot for Post-Micellar C9-7EO Aqueous Concentration.....	22
	Regressed Model (Accepted Model)	
8.	Residuals Plot for Post-Micellar C9-7EO Aqueous.....	22
	Concentration Regressed Model (Accepted Model)	
9.	Dynamic Surface Tension of C9-7EO in Water as a Function.....	27
	of Surface Age	
10.	Plot of Linear Dynamic Surface Tension Variance from.....	28
	Diffusion Ideality as a Function of Surface Age	
11.	Residuals Plot for C9-7EO Regression for Diffusion.....	29
	Coefficient (Surface Age < 5 Seconds)	
12.	Prediction Plot for C9-7EO Regression for Diffusion.....	29
	Coefficient (Surface Age < 5 Seconds)	
13.	Residuals Plot for C9-7EO Regression for Adsorption.....	31
	Coefficient (Surface Age > 6 Seconds)	
14.	Graphical Determination of Demicellization Constant.....	34

15. Critical Micelle Concentration as a Function of.....	39
(Ionic Radius)*(Total M of Ions)	
16. Rate of Demicellization as a Function of Concentration.....	42

LIST OF TABLES

1. Coefficients for Estimated Models for Pre-Micellar.....	17
Behavior of C9-7EO in Water	
2. Coefficients for Estimated Models for Post-Micellar.....	21
Behavior of C9-7EO in Water	
3. Critical Micelle Concentrations and Equilibrium Surface.....	23
Tensions at CMC for Solutions of C9-7EO	
4. Surface Concentration and Occupied Surface Area for.....	24
C9-7EO in Solution	
5. Free Energies of Adsorption and Micellization for C9-7EO.....	25
6. Coefficients for Estimated Models Providing the Diffusion.....	30
Coefficient of C9-7EO in Water	
7. Coefficients for Estimated Models Providing the Adsorption.....	32
Coefficient of C9-7EO in Water	
8. Diffusion and Adsorption Coefficients with Energy of.....	33
Adsorption for C9-7EO Solutions.	
9. Demicellization Rate Constants for Aqueous Concentrations.....	35
of C9-7EO.	
10. Demicellization Rate Constants for Various Concentrations.....	36
and Solutions of C9-7EO	
11. Basic Properties of Salts Employed in This Study.....	37
12. Number and Size of Ions in Each Salt Solution.....	39

ABSTRACT

The dynamic and equilibrium surface tensions of a nonionic surfactant not previously available to industry, septaethyleneglycol monononyl ether (C9-7EO), were measured in pure water and with various salts. Experimental results indicate that the adsorption mechanism is primarily diffusion-controlled and is noticeably affected by the presence of inorganic salts. A thorough examination at a number of concentrations yields free energies of adsorption and micellization, surface concentration, and the rate of demicellization in concentrated solutions. Although the salt solutions lower the free energy of adsorption significantly, the salts also act to stabilize micellar aggregates which may have a detrimental effect on a desired detergency process.

CHAPTER 1

INTRODUCTION

Many metric tons of synthetic surfactants are consumed annually in the production of aqueous detergent compounds that are then used to clean numerous substrates of still more numerous soils.¹ Despite the variety of soil/substrate combinations that are cleaned, the general formula for cleaning any hard surface is generally the same, which is to incorporate these synthetic surfactants with various inorganic and organic salts, generally termed “builders.”^{1,2} The benefit of this combination is to capitalize upon the capacity of a surfactant to wet soils and surfaces, emulsify oily materials, and suspend removed soils as well as the builder’s provision of an alkaline medium for the neutralization of acidic soils (cleaners utilized in household and institutional environments are typically basic, although acid pH cleaners do fulfill certain specialized roles), deflocculation of soils, and chelation of minerals.^{3,2,4}

The surfactant-detergent combination is generally synergistic in that the two mechanisms of cleaning are convergent in result, yet dissimilar in action.^{5,4} Evidence has emerged over the past few decades that such synergistic benefits may go beyond the simple concept of multiple pathways to a goal and physicochemical interactions between the surfactant and builders have been identified, particularly as relating to aggregation characteristics of the surfactants.^{6,1,5} The kinetics of surfactant aggregation have direct bearing on the action of soil removal and, significantly, the micellar breakup or relaxation has been directly correlated to effectiveness in detergency.⁷

Historical studies have focused on the interplay between ionic surfactants and builders only to a limited degree and much more work has been done in controlled circumstances with simple salts to minimize effects other than charge interaction.^{6,1,3} The benefit of this approach has been the development of clear ideas regarding charge interaction and how the physical properties of ionic amphiphiles may change as a result. These studies are often improved upon through the addition of nonionic surfactants in order to gain better understanding of more complex “mixed surfactant” systems such as what is typically

used in a formulated cleaning product,^{6,1} but the literature is rather lacking in information relating the responses of purely nonionic surfactant systems to ionic effects and especially in the examination of more complex salts typical of builders.

It is known that ionic materials will impact the behavior of nonionic surfactants, and the typical explanation is the phenomenon of “salting out” or “salting in;” solubilities change according to the ions in solution because of how the water organized by a surfactant hydrophile interacts with these ions.⁶ The surfactant solubility is directly tied to aggregation properties, but hard relationships relating industrial nonionic surfactants, salt properties (e.g., ionic strength of solution and ion size), and dynamic characteristics are limited.^{1,3}

Further complicating the attempts to build a concise picture of cause and effect is the polydispersity of typical industrial nonionic surfactants.⁸ Cost effective manufacturing techniques result in a broad distribution of ethoxomers as well as a significant amount of unreacted base alcohol (see Chart 1). A clear thermodynamic model is best established with discrete materials and it is this approach that much research takes. Unfortunately, a model built upon a single moiety provides little clarity when industrial grade surfactants are considered.

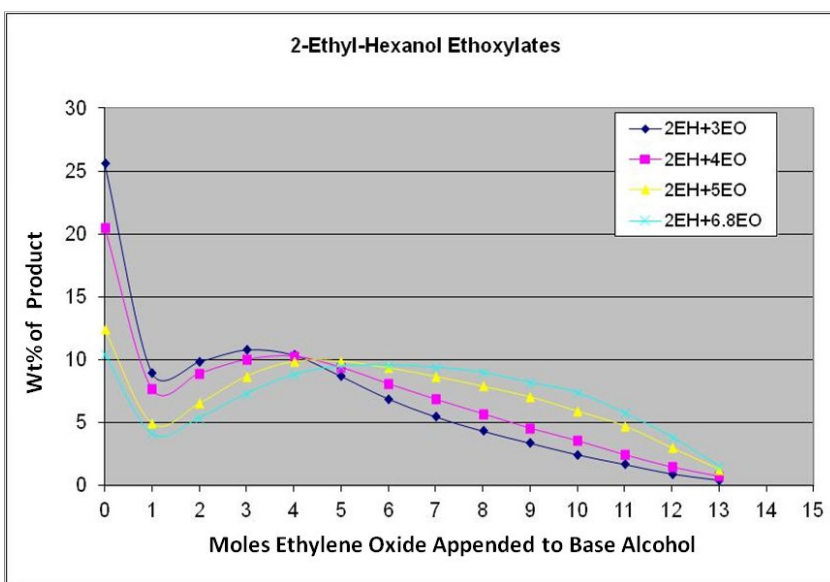


Chart 1. Relative Percentages of Ethylene Oxide Adducts for Industrial 2-Ethylhexanol Ethoxylates

Considering that aggregation, particularly formation and relaxation of micelles, has been tied directly to detergency,⁷ how ionic materials impact aggregation characteristics of industrial surfactants is of significant interest to those working to develop more efficient cleaning formulas. Although it may be difficult to build a thermodynamic model upon specific materials that contain numerous moieties, the functional aspects may be explored by examining physical and thermodynamic aspects of nonionic surfactants and how they are influenced by various ions.

CHAPTER 2

THEORETICAL FRAMEWORK

The amphiphilic nature of surfactants are well known to be responsible for their unique surface and aggregation characteristics.⁶ The resulting interactions among surfactant monomers and with the environment at hand are often easily understood from an anecdotal approach. Simply put, one side of a surfactant monomer in solution prefers not to associate with the solvent and the other side prefers to mix completely into solution. All surfactant interactions being explained to novices begin with this simple story, but the details of this dual nature quickly become complicated. Multi-volume book sets have been published to deal with the kinetic and thermodynamic aspects of only small sets of surfactants, so it is quite a bit beyond the scope of this paper to provide a thorough treatment of aspects of surfactant interaction.⁹

In this theoretical exploration very specific attributes of aggregation will be discussed with the aid of mathematical relationships that have been developed over nearly half a century. The goal in this treatment is primarily to explain why the research took the direction that it did. In short, a large amount of information available to describe surface aggregation and how micellar formation and relaxation impacts that behavior is distilled into a few relationships. In this way information about aggregation becomes immediately accessible through experimental methods.

2.1 THE IMPORTANCE OF MICELLAR RELAXATION TIME

All surfactants in solution exhibit a 3-way equilibrium among monomer, micellar, and adsorbed layer states.¹⁰ This equilibrium is constant, but not static, with a continual flux among the three “phases” (Figure 1). The flux is characterized by the rate of adsorption/desorption of the surfactant at an available interface and two relaxation times for the micelles.^{10,11} The first micellar relaxation time is known as the fast relaxation time (τ_1), which is the time that it takes for a surfactant monomer to exit the micelle and

enter the bulk solution. The second relaxation time is the slow relaxation time (τ_2), which is the time that it takes for the micelle to degrade completely.¹²

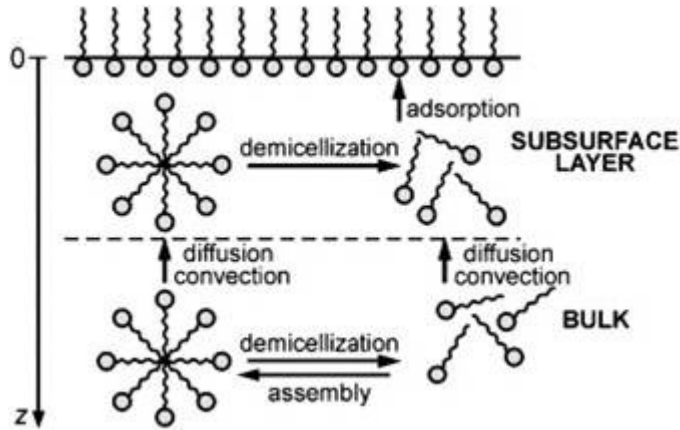


Figure 1. Illustration of Surfactant States at Solutions Equilibrium¹⁰

It has been shown that more stable micelles contribute to longer wetting times, lower amounts of foam generation, and more rapid solubilization of oil.¹² All of these attributes may be traced directly to the flux of the surfactant monomer to the interface, indicating that micelles affect the adsorbed layer indirectly by limiting the amount of surfactant available to move to an interface. In this way, more stable micelles contribute to higher dynamic surface tension (DST) as seen in a bubble tensiometer.¹³

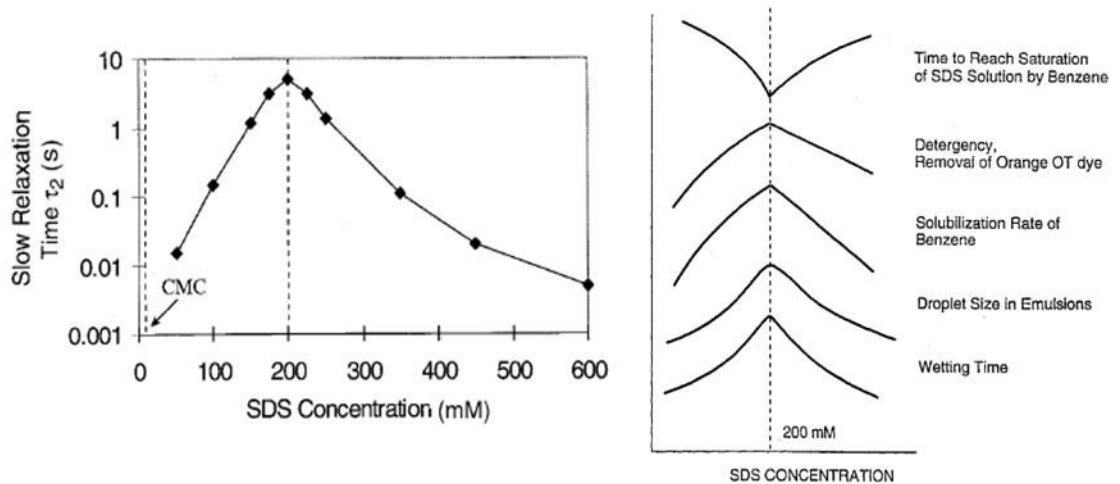


Figure 2. Maximal Micelle Stability for Sodium Dodecylsulfonate Juxtaposed with Performance Properties¹²

If relaxation time is the key to properties that are generally seen as indicative of cleaning processes (e.g. foaming and wetting), then maximizing the relaxation time should similarly show maxima/minima for other properties. It is interesting to note that this idea is unambiguous when examining various performance properties of a commonly used industrial surfactant, sodium dodecylsulfate (SDS), in light of micellar relaxation time (Figure 2).¹²

2.2 DESCRIBING SURFACTANT MIGRATION TO AN INTERFACE

It must be emphasized that the processes described above are not affected by micellar relaxation in a direct manner; rather it is the impact of micellar relaxation on surfactant transport to an interface. Referring again to Figure 1, two regions are identified within a solution. The first is the subsurface layer from which surfactants will move to adsorb at the interface and which is subsequently depleted of surfactant. The second region is the bulk from which new surfactant monomer must come to restore the concentration of the subsurface. When there are no micelles present (i.e., below the critical micelle concentration or CMC), the process of restoring concentration to the subsurface is determined solely by diffusion and is a relatively fast process.¹⁴ Above the CMC the influence of micelles must be considered as these structures may hold the majority of surfactant concentration within the bulk.

The Ward-Tordai equation describes the time dependency of adsorption as follows:¹⁵

$$\Gamma^H(t) = 2C_0 \left(\frac{Dt}{\pi}\right)^{\frac{1}{2}} - 2 \left(\frac{D}{\pi}\right)^{\frac{1}{2}} \int_0^t C_s(t-\tau) d\tau^{\frac{1}{2}} \quad (1)$$

in which C_0 and C_s are the bulk and subsurface concentrations of surfactant, respectively; D is the surfactant diffusion coefficient; $\Gamma^H(t)$ is the surface density; t is the time; and τ is a dummy time delay variable. The adsorption equation at constant temperature and pressure relates the changing subsurface concentration to a varying or dynamic surface tension ($\gamma(t)$) through surface adsorption:¹⁶

$$d\gamma(t) = -\frac{RT\Gamma^H(t)}{C_s} dC_s \quad (2)$$

In this case R represents the gas law constant and T represents temperature. Utilizing the two equations allows the interrelation of dynamic surface tension, concentration within the bulk and at the subsurface region, and diffusion of surfactants to an interface.

Examining a system below the CMC allows one to ignore micellar effects and decreasing concentration allows further simplification because as $C_0 \rightarrow 0$, $C_s \approx C_0$. Real world results compared to the simplified Ward-Tordai model at concentrations below the CMC have indicated that two processes exist in the movement of surfactant to the interface. The “short time” process is simply the diffusion of surfactant monomer within the solution and the “long time” process involves overcoming an activation energy related to crowding or repulsion of surfactant at the interface. This second process is related to the change in free energy due to increased order at the interface, overcoming the headgroup interactions of surfactants (which is less of a concern for nonionic systems), and crowding at the interface. By assigning the two processes two diffusion coefficients the Ward-Tordai equation may be separated into two reduced equations:^{16,17,18}

$$\gamma_{t \rightarrow 0} = \gamma_0 - 2RTC_0 \sqrt{\frac{D_d t}{\pi}} \quad (3)$$

And

$$\gamma_{t \rightarrow \infty} = \gamma_{eq} + \frac{RT\Gamma_{eq}^2}{C_0} \sqrt{\frac{1}{\pi D_a t}} \quad (4)$$

in which γ_t is the dynamic surface tension at surface age, t; γ_0 is the surface tension of the solvent; and γ_{eq} is the equilibrium surface tension. Γ_{eq} is the surface density at equilibrium for that concentration of surfactant. The terms D_d and D_a respectively represent the diffusion coefficient related to simple diffusion through the solution and the adsorption to the surface from the subsurface layer by a surfactant monomer, also referred to as the effective adsorption coefficient.¹⁸

Under ideal circumstances, utilizing the D_d and D_a will allow one to determine the actual energy barrier involved in adsorbing to the surface through equation (5), which describes the effect of adsorption energy upon the observed diffusion coefficient.¹⁶

$$D_a = D_d * \exp\left(-\frac{2E_a}{kT}\right) \quad (5)$$

In this last equation, E_a is the adsorption energy and k is Boltzmann's constant.

2.3 MICELLAR IMPACT UPON ADSORPTION

Equation (4) has been used successfully in concentrations both above and below the CMC, although the value of D_a will shift. This shift is related to the process of demicellization and can be taken as a whole as opposed to looking individually at the relaxation times. Kjellin et al., found that the adsorption coefficient could be fit to both pre- and post-micellar systems. In exploring this possibility Rillaerts and Joos obtained this variation upon (4):^{19,16,18}

$$\gamma_{t \rightarrow \infty} = \gamma_{eq} + \frac{RT\Gamma_m^2}{2c_0t} \sqrt{\frac{1}{D_a k}} \quad (6)$$

In this case k is assigned the role of the overall rate constant for demicellization. In this way it is implied that obtaining D_a outside of a micellar system allows the impact of micellar relaxation to be seen as a function of dynamic surface tension by reapplying the found value to a micellar system. Although it is common to fit even complex relationships with a first order reaction rate as long as the applied shift in a system is minimal, having three independent effects (diffusion, adsorption, and demicellization) taxes dynamic experimentation beyond linearity.¹⁸

Thankfully, Rillaerts and Joos also understood this to be the case and proposed the use of surface dilatation (θ , the stretching of an interface) in conjunction with Ward and Tordai's relationship to describe the impact of demicellization. Stating that the penetration depth of a zone depleted of surfactant monomer at the site of the dilatation is described as:

$$\delta = \left(\frac{\pi D_d}{2\theta} \right)^{\frac{1}{2}} \quad (7)$$

in which θ is estimated as $1/2t$, it may be seen that a theoretical zone is constructed without a concentration, but with a flux provided by the diffusion coefficient. Using the depletion zone behind the dilatation (δ) as a variable, another variant of the Ward-Tordai relationship is substituted from:¹⁹

$$\gamma_{t \rightarrow 0} = \gamma_0 - \Gamma_{\text{eq}} \frac{d\gamma}{dC} * \frac{\theta}{(Dk)^{\frac{1}{2}}} \quad (8)$$

to:

$$\gamma_{t \rightarrow 0} = \gamma_0 - \Gamma_{\text{eq}} \frac{d\gamma}{d\delta} * \frac{\theta}{(Dk)^{\frac{1}{2}}} \quad (9)$$

As will be shown, this is a simpler approach due to many of the variables cancelling during solution. Thus even without a complete model demonstrating fast and slow relaxation times, the changes within a system that act to speed or slow the relaxation may be observed. Rate constants calculated in this manner have been comparable to those calculated by other methods such as pressure and temperature jumps.¹⁴

CHAPTER 3

MATERIALS AND METHODS

3.1 CHEMICALS

Unless otherwise specified, the chemicals used in this study were reagent grade, obtained from Sigma-Aldrich (St. Louis, MO), used as received. Water was HPLC Chromasolve grade (certified $\leq 0.0001\%$ impurities) also obtained from Sigma-Aldrich. The nonionic surfactant studied was a broad-range nonanol ethoxylate. The Air Products New Product Research Group obtained the base alcohol (85% 1-nonanol, 15% 2-nonanol, provided as Neodol 9, used as received) from Shell Chemical and added 7 molar equivalents of ethylene oxide via base catalysis (45% KOH followed by a low-pressure water strip to ensure anhydrous starting material). This methodology is well known in industry and documented elsewhere.²⁰ The resulting surfactant was analyzed via nuclear magnetic resonance (NMR) and matrix-assisted laser desorption/ionization (MALDI) to produce the profile shown in Chart 2.

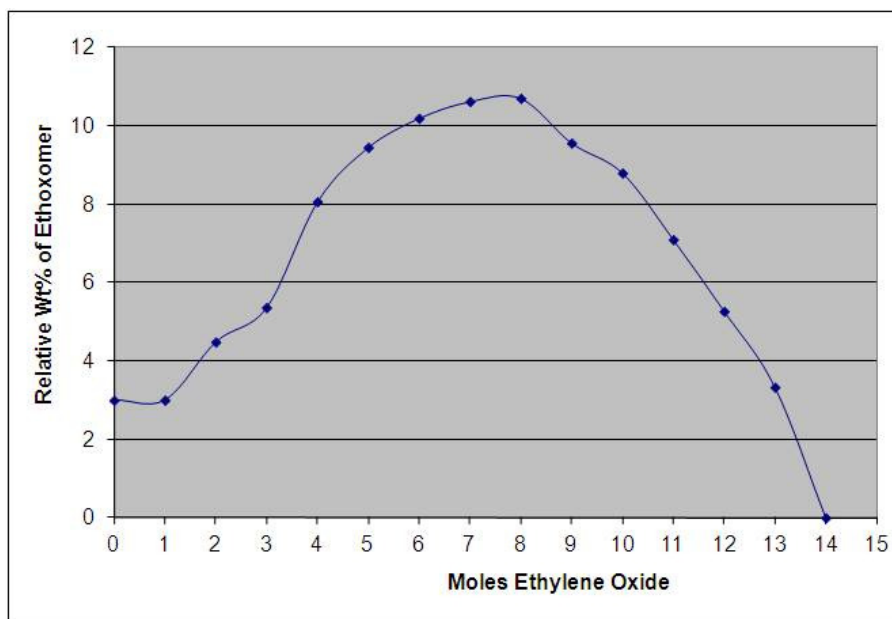


Chart 2. Relative Distribution of Ethoxymers Present in the Nonionic Surfactant Studied (C9-7EO)

The surfactant (C9-7EO) was further purified upon receipt via the three-phase extraction technique commonly referred to as 3PHEX.²¹ Briefly, equal weight amounts of n-hexane and water are combined and surfactant in the amount of 15% of the total mass is then added. The container is closed and magnetically stirred while immersed in a water bath to equilibrate to an initial temperature (in this case T_I was 30° C). The stirrer is turned off and two phases, an organic solvent (or oil) phase and an aqueous phase, quickly coalesce. At this first temperature, the aqueous phase is a microemulsion of oil in a continuous water phase, stabilized by the surfactant. Ideally, the oil soluble impurities primarily reside within the oil phase. The oil phase is drawn off and replaced by an equal amount of fresh hexane and the container is closed and returned to the water bath and stirred. This time the temperature is allowed to equilibrate at a higher temperature (T_{II} in this case was 65° C), the stirrer is again turned off and the two phases coalesce. In this second case the oil phase is a water in continuous oil phase microemulsion and the aqueous phase contains the water soluble impurities. The aqueous phase is drawn off and replaced with an equal amount of fresh water.

This purification may proceed stepwise for a number of iterations but these steps were only carried out twice each for the C9-7EO. The final step is to allow equilibration at a mid-range temperature (T_{III} in this case was 50° C), which results in three phases, with the purified surfactant forming the greatest part of the middle phase. The aqueous and oil phases are drawn off and the surfactant is dried by heating at 50° C under a mild vacuum (gradually increasing to 20 in Hg). The purified surfactant was checked to ensure that the mean ethoxylation range had not shifted significantly through the use of a cloudpoint test. (The range was also verified via NMR, GC-FID and MALDI for the benefit of other Air Products researchers working with this material, but that was outside of this study.)

Household formulated cleaning products generally employ 2 - 6 wt% of ionic salts as builders.^{3,2} Using NaCl as a representative “builder,” 3 wt% becomes roughly 0.5 M. All solutions were thus employed at 0.5 M so that a standard molar concentration could be established as a baseline in terms of relative concentrations. The 0.5 molar solutions were prepared in the typical manner utilizing volumetric glassware. 5 wt% surfactant

solutions were prepared in pure water, as well as each salt, to provide a stock solution that was further diluted into either water or the given salt solution. In this way the salt concentration varied minimally regardless of the level of surfactant. The pH was checked for each solution so that pH impact could be observed as well.

Three additional CaCl_2 solutions were prepared with an addition of either HCl or $\text{Ca}(\text{OH})_2$ to adjust the pH with minimal impact upon the predominant ions.

3.2 HIGH THROUGHPUT SAMPLE PREPARATION

A Perkin-Elmer JANUS Automated Workstation (Janus) was employed to prepare the high number of samples which would be required for this study. Details regarding how this system was employed and standardized are provided in Appendix A (use in preparation of test solutions) and Appendix B (establishment of a photometric method to eliminate probable outliers). Briefly, the Janus has the capability of preparing 48 solutions with a high degree of confidence within 8 - 15 minutes. This is done through the employment of robotic arms and automated syringe pumps fitted with disposable pipette tips. Although stock solutions of surfactants were manually prepared to ensure accuracy not obtainable with the Janus, aqueous dilutions were then prepared with the high throughput system. To further improve upon accuracy, gross outliers were identified and removed via image analysis (see Appendix B).

3.3 INSTRUMENTATION AND SOFTWARE

Equilibrium Surface Tension

A Krüss K12 tensiometer with a roughened platinum (Wilhelmy) plate attached to a precision internal balance was used for measuring equilibrium surface tension (EST) of surfactant solutions via standard method.¹⁵ All samples were prepared in uniform jars with attention paid to maintaining nearly the same volume for each. Samples were equilibrated in a $25 \pm 0.04^\circ \text{C}$ water bath and the tensiometer employed a recirculating flow from the same bath to maintain a constant temperature in the sample well.

Control of the instrument was maintained through the Krüss LabDesk software and measurements were taken continuously until the change noted among 5 sequential readings was less than 0.01 dyne/cm (mN/m). This allowed proper time for equilibration of the solution with the plate and ensured that the precision balance had minimized oscillation.

Dynamic Surface Tension

A Krüss BP2 tensiometer utilizing the maximum bubble pressure method was employed for the determination of dynamic surface tension (DST) of surfactant solutions.¹⁴ All samples were prepared in jars of the same dimensions with care taken to ensure that the same approximate volume was maintained. Samples were equilibrated in a $25 \pm 0.04^\circ \text{C}$ water bath and the same temperature was maintained in the sample well. Flow rate of the nitrogen supplied through the capillary was varied so that changes in surface tension as a function of surface age could be observed. Data was acquired through the use of Krüss LabDesk software.

Data Analysis and Treatment

Microsoft Excel was used for the aggregation of data and execution of most simple calculations. Tableau 6.1.2 (Tableau Software, Inc., Seattle, WA) was employed for analysis of trends, development of concepts regarding relationships of variables, and simple regressions. The strength of Tableau is that a simple “point-and-click” interface allows a rapid development of a structure similar to an Excel pivot-table with very little effort. Stat-Studio 8.2 (Air Products and Chemicals, Inc., Allentown, PA) is a proprietary software package with powerful modeling, projection, and experimental design modules. In this case Stat-Studio was used for the development of regression curves to solve linear equations employing experimental data as variable sets. LMMPro 1.06 (C.P. Schulthess with Alfisol, LLC, Coventry, CT) was used in casting Langmuir isotherms to validate concentration effects upon physical responses to testing.

CHAPTER 4

EXPERIMENTAL PROCESS AND RESULTS

Each surfactant-salt system (or surfactant in pure water) was taken through the same process described below as the study proceeded. By way of illustration, detailed explanation of the experimental methods and analysis employed for one type of solution is provided below, that of the C9-7EO in pure water. It would be redundant and of limited value to go through the process involved with each surfactant/solution in terms of experimental process, so complete results are provided as a summary following the single examination provided in detail. In all cases the process was typical of the example given. Data analysis methods are described in detail once for the sake of clarity, but it is safe to assume that each method was employed numerous times although not mentioned specifically again (e.g., the Grubb's Test is explained once but it was used frequently in qualifying questionable data points).

4.1 CRITICAL MICELLE CONCENTRATION

A series of dilutions were prepared that encompassed the anticipated CMC. Equilibrium surface tensions for these solutions were obtained through the use of the Krüss K12 tensiometer as described above. The measurements were plotted against the surfactant concentration to produce graphs of the type shown in Chart 2. The purpose of these initial plots was to gain a general idea of the range for the CMC and to aid in the linear regression employed to develop lines describing the relationship between post-micellar and pre-micellar concentrations and surface tension.

Even without the calculations to develop a line the linear nature of both sides of the CMC is easily seen by eye. Despite the 3PHEX purification process there is a slight characteristic "bulge" below the CMC/EST range due to impurities within the surfactant. These impurities will impact surface characteristics at the point at which excess surface concentration of the surfactant is first attained and might interfere with the proper development of the linear equation. To further add to the difficulties, surface flux

resulting from an increase in bulk surfactant concentration beyond the CMC prevents the attainment of a flat line for the post-micellar concentration. The estimation of a proper line is thus somewhat complicated in many cases.^{15,6,21}

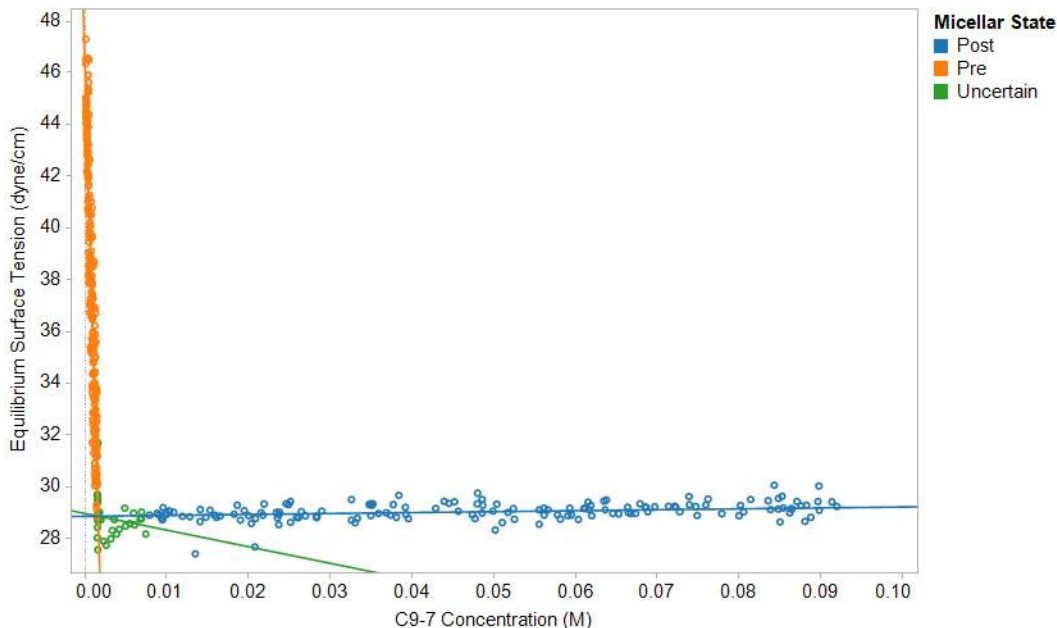


Chart 3. Equilibrium Surface Tension as a Function of C9-7EO Concentration in Water

In the case of the pre-micellar concentration, the process was rather simplified thanks to the surprisingly consistent nature of the data. By visually estimating the surface tension at the CMC in accordance with the line which would be developed from the post CMC data, one could see that values above 29 dyne/cm that occur when the concentration is less than 0.004 M are most likely “pre-micellar.” Assigning that term differentiated those points from the remainder. It is also known that the pre-micellar behavior of surfactants cannot be accurately modeled to pass through the EST of water at a concentration approaching 0 M, so some points that could be discarded at the lowest concentrations as well. Typical surfactant behavior indicates that linear behavior is attained beyond the so-called C_{20} (the concentration at which the surface tension of water is reduced by 20 dyne/cm)⁶ and it may be seen that this particular data set actually begins at a surface tension below that point. Analytical tools could also be utilized to show the accuracy of the estimated model and those were employed as described below.

Linear regression to fit the estimated model:

$$\text{EST (dyne/cm)} = m * \text{Concentration (M)} + b$$

was performed through the statistical and modeling software, Stat-Studio. The first regression provided a root mean square error (RMSE) of 1.76 and a correlation coefficient (R^2) of 0.862. It is possible that the data obtained was not completely within the linear region of the CMC curve and this possibility was checked by eliminating the lowest 4 concentrations to determine if the error decreases and/or the correlation improved. Continuing with this method of estimating the value of the generated models was easily done and so a number of sets were generated for evaluation. The results of these sets are shown in Table 1.

Table 1. Estimated Models for Pre-Micellar Surfactant Behavior, C9-7EO in Water

Excluded Points		Relative Error (RMSE)	Correlation (R^2)	Significance (p)	Slope (m)	Intercept (b)
None		1.757	0.8622	<0.0001	-9025	46.84
Lowest Conc.	4	1.762	0.8554	<0.0001	-8950	46.74
	8	1.777	0.8491	<0.0001	-8950	46.74
	12	1.792	0.8427	<0.0001	-8950	46.74
Highest Conc.	4	1.772	0.8568	<0.0001	-9017	46.83
	8	1.768	0.8555	<0.0001	-9074	46.87
	12	1.766	0.8535	<0.0001	-9132	46.91
Lowest/Highest*	4	1.777	0.8496	<0.0001	-8942	46.73
	8	1.789	0.8416	<0.0001	-9000	46.78
	12	1.804	0.8323	<0.0001	-9066	46.83

*In these data sets, the nominal points were excluded from both the lowest and highest concentrations.

The coefficients shown in Table 1 indicated that the pre-micellar data was extraordinarily well behaved and only minimal changes in the estimated model occurred in the course of excluding data points from either the upper or lower concentrations. Although the RMSE increased and the correlation decreased for the exclusion of the lowest 4, 8, and 12 points, the fact that the slope and intercept (m and b, respectively) did not change within the reported significant figures indicated that these values may be nearer to the “truth” than keeping all data points.²²

Examining the resulting prediction plot for the accepted model (Chart 3) gives some clue as to why there is such a difference in effect when excluding top and bottom points. At the lower end of the concentration spectrum are a few high leverage points followed immediately by a number of low leverage points. At the higher end of the concentration, on the other hand, many of the points show high leverage which would result in an overall shifting of the model when those points are excluded. Based on this observation as well as the overall scatter of the residuals plot (Chart 4), it was decided to use the highlighted model with m and b coefficients of -8950 and 46.74 , respectively.

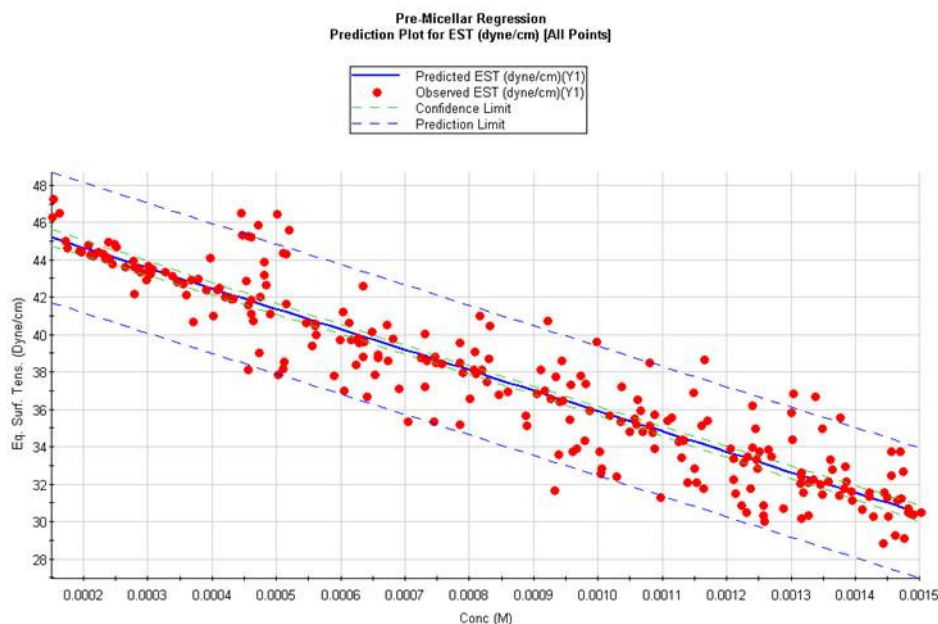


Chart 4. Prediction Plot for Pre-Micellar C9-7EO Aqueous Concentration Regressed Model (All Data Retained)

Estimating the model for the post-micellar line was expected to be more difficult because the data was clearly not as well behaved. Furthermore, the lack of cohesiveness due to the presence of impurities made it difficult to determine at what concentration to begin the data set. This last issue was actually critical to the development of a good model as the increased flux resulting from higher concentrations of surfactant would skew the EST and introduce greater uncertainty into the model. For this reason, the first regression used data which appeared to be rooted in the area demonstrating surface active effects for the

impurities. Unsurprisingly the first regression showed a significant lack of correlation. (These results may be seen in Table 2 as the row with no excluded points).

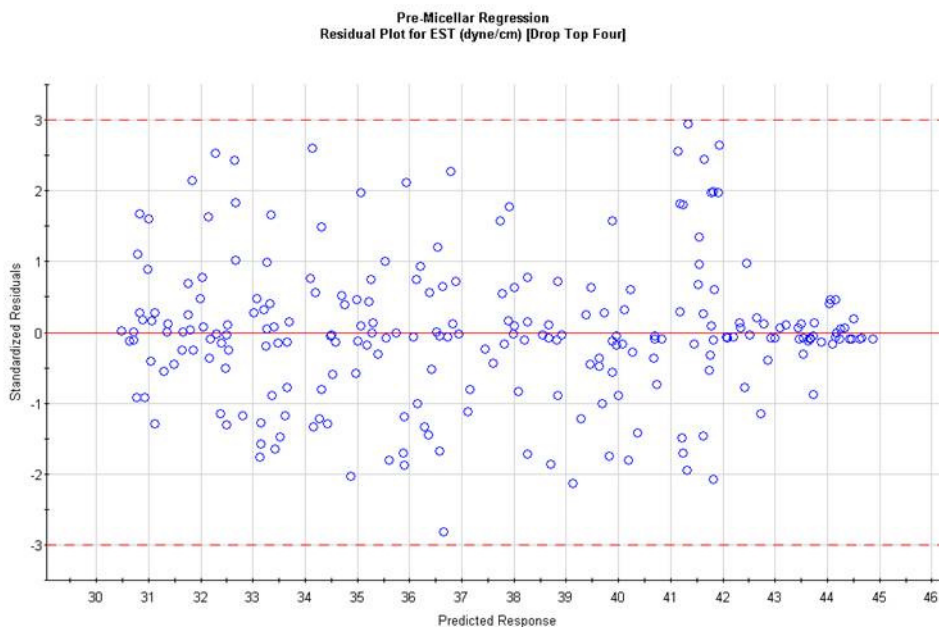


Chart 5. Residuals Plot for Pre-Micellar C9-7EO Aqueous Concentration Regressed Model (Accepted Model)

Before moving ahead with the systematic exclusion of the high and low concentration levels, attention should be paid to the initial plot that encompasses all of the data. There are four points in particular that appear to be outside the range of the rest of the data, and these are indicated with red circles in a close-up view of Chart 2 shown below as Chart 5. By determining the maximum normalized residual for those points (i.e. the Grubb's Test), a confident determination could be made regarding whether or not those points were truly part of the data set or outliers.^{22,23} Even though the proper assumption in using the Grubb's Test is that there is only one possible outlier (the one being tested), the large number of data points again simplified the method by providing a basis that easily overwhelmed the potential error of keeping 3 other data points that are not necessarily part of the population.

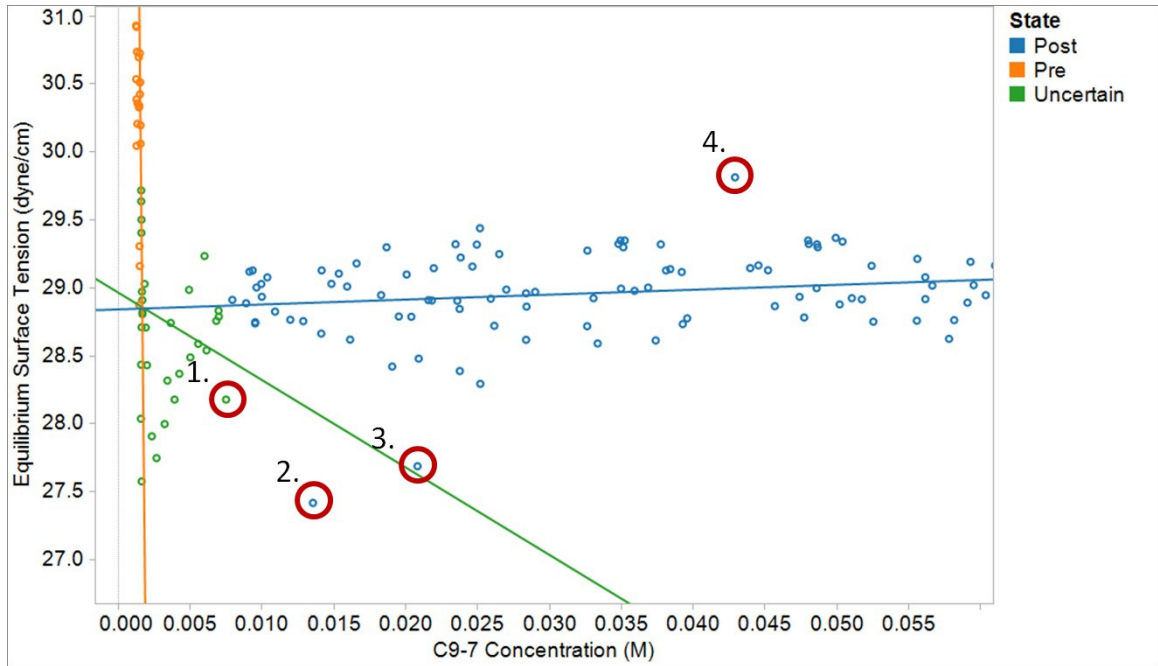


Chart 6. Examination of Potentially Erroneous Points Identified from Chart 3

The equation for the Grubb's Test is generally:²³

$$G = \frac{|Y_i - \bar{Y}|}{s} \quad (10)$$

and the null hypothesis is rejected if:

$$G > \frac{N-1}{\sqrt{N}} * \sqrt{\frac{\left(t_{\frac{\alpha}{2N}, N-2}\right)^2}{N-2 + \left(t_{\frac{\alpha}{2N}, N-2}\right)^2}} \quad (11)$$

In the above equations, Y_i is the questionable point, \bar{Y} is the mean of the sample, s is the standard deviation of the sample, N represents the number of samples, and $t_{\alpha/2N, N-2}$ is the critical value of the t-distribution at $\alpha/2N$ at $N-2$ degrees of freedom (α being the confidence level). In this way points labeled as 2, 3, and 4 in Chart 5 are identified as questionable within a 99% confidence level and excluded from the data set although point 1 is embraced.

With the new data set the regression was performed again, this time with slightly better RMSE and correlation, although still far from ideal. The 4 lowest concentrations were

excluded and the model improved again, but that was the best correlation and error obtained (see Table 2). Although this was somewhat bothersome, two facts allow for the acceptance of the post-micellar model. The first was that although the model was poorly correlated, the relative error was actually quite small and gave confidence that the intercept is a good approximation of the EST at the CMC (γ_m). The second was that in the method of calculating the CMC (solving the two lines for a single point) the effect of the post-micellar slope is miniscule compared to the more consistent data that describes the pre-micellar line. In other words, even significant changes in the slope and intercept for the post micellar line had a small effect on the final calculated CMC. This last was reflected through the propagation of error and is represented in the chart of all CMC values as the greatest source of uncertainty in the summary, Table 3.

Table 2. Estimated Models for Post-Micellar Surfactant Behavior, C9-7EO in Water

Excluded Points		Relative Error (RMSE)	Correlation (R^2)	Significance (p)	Slope (m)	Intercept (b)
None		0.5099	0.0650	0.0006	3.902	28.78
Identified Outliers		0.3689	0.1577	<0.0001	4.646	28.79
Lowest Conc.	4	0.2990	0.2647	<0.0001	5.346	28.47
	8	0.2943	0.2508	<0.0001	5.160	28.76
	12	0.2763	0.2146	<0.0001	4.451	28.81
	16	0.2691	0.1894	<0.0001	4.085	28.24
Highest Conc.	4	0.2967	0.2466	<0.0001	5.182	28.75
	8	0.2933	0.2656	<0.0001	5.523	28.74
	12	0.2956	0.2578	<0.0001	5.565	28.74
Lowest/Highest*	4	0.2879	0.2177	<0.0001	4.720	28.79
	8	0.2625	0.1969	<0.0001	4.224	28.84
	12	0.2631	0.1787	<0.0001	4.141	28.84

*In these data sets, the nominal points were excluded from both the lowest and highest concentrations.

In the process of establishing that the model is useful, the normal probability plot was examined (Chart 7) and it was seen that although the model has poor correlation, it still approximated a normal distribution. Similarly, the residuals plot (Chart 8) showed through random scatter that the model estimate does follow a linear relationship.

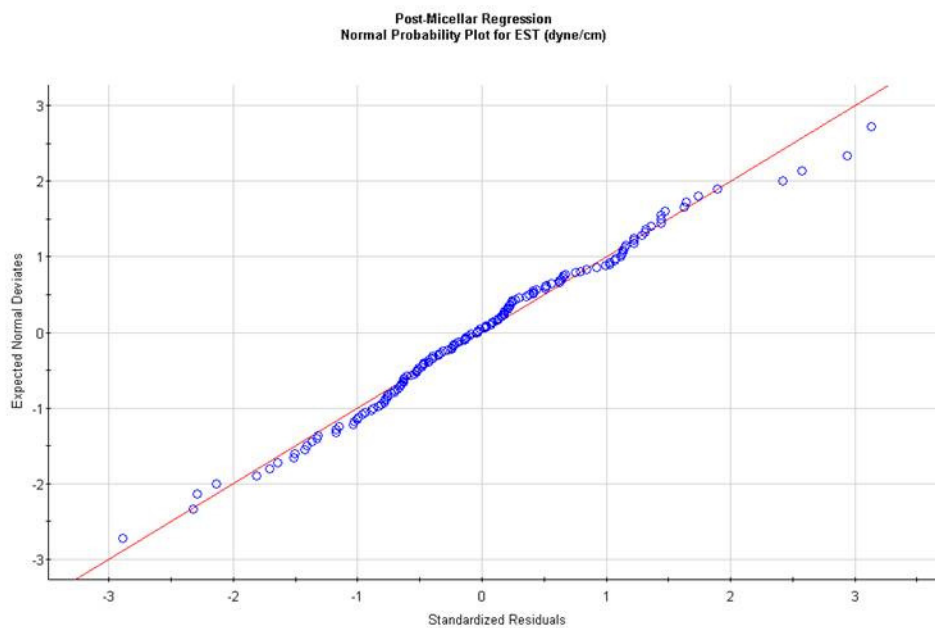


Chart 7. Normal Plot for Post-Micellar C9-7EO Aqueous Concentration Regressed Model (Accepted Model)

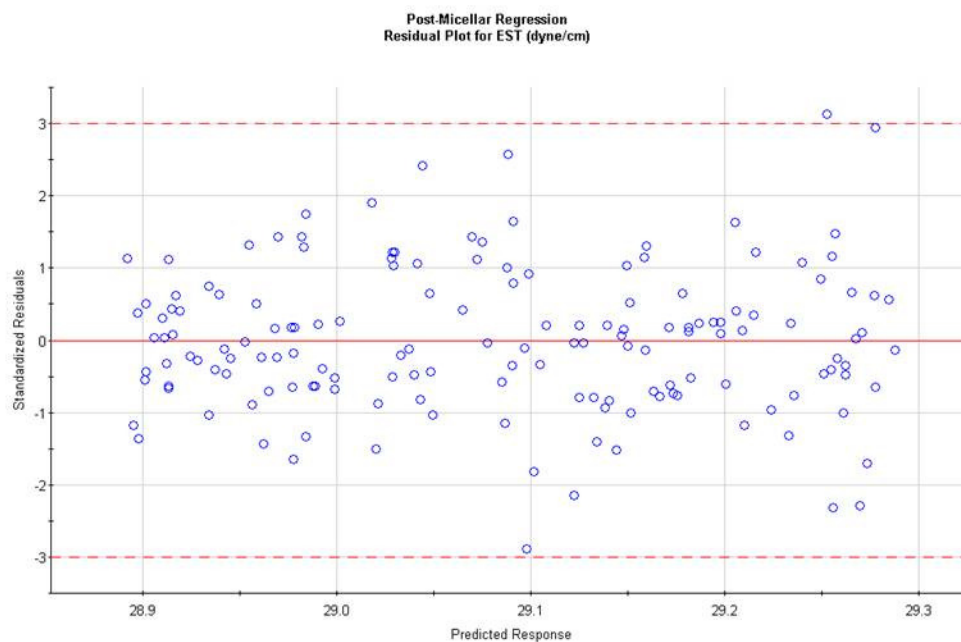


Chart 8. Residuals Plot for Post-Micellar C9-7EO Aqueous Concentration Regressed Model (Accepted Model)

In the same way, all solutions were examined to determine the best model for pre- and post micellar behavior.

By substituting the coefficients obtained into the linear models for pre- and post-micellar surface tension and setting the equations equal to each other, a trivial solution resulted in a concentration of 2.01×10^{-3} M, the CMC, producing a surface tension (γ_m) of 28.7 dyne/cm. These are values that are in reasonable agreement with similar materials tested in the literature. Table 3 shows the obtained values for this and similar surfactants in pure water along with all determined values for the various salt solutions tested.

Table 3. Critical Micelle Concentration and Equilibrium Surface Tension for C9-7EO

Solution	pH	Critical Micelle Concentration (CMC)		Equilibrium Surface Tension (EST) at CMC	
		mol/L (*10 ³)	Error (*10 ³)	dyne/cm	Error
Water	7.0	2.01	0.21	28.7	0.45
0.5M NaCl	6.9	0.730	0.064	28.5	0.15
0.5M KI	6.9	1.14	0.092	28.4	0.34
0.5M MgSO4	6.2	0.774	0.12	28.3	0.040
0.5M Na ₂ SO4	6.8	0.337	0.034	28.7	0.28
0.5M CaCl ₂	6.4	0.933	0.072	27.9	0.030
0.5M CaCl ₂	4.1	0.873	0.072	28.3	0.31
0.5M CaCl ₂	9.7	0.807	0.068	28.2	0.30
0.5M CaCl ₂	10.3	0.914	0.070	28.3	0.28

4.2 SURFACE EXCESS CONCENTRATION

The surface concentration of surfactant at the CMC is given by the Gibbs Adsorption equation:⁶

$$\Gamma_m = -(RT)^{-1} * \left(\frac{\partial \gamma_{LV}}{\partial \ln c} \right)_T \quad (12)$$

in which R is the gas constant, T is the absolute temperature, γ_{LV} is the surface tension at the air-water interface, and C is the molar concentration of surfactant. This equation may be simplified mathematically to incorporate a base-10 log as follows:⁶

$$\Gamma_m = -(2.303RT)^{-1} * \left(\frac{\partial \gamma_{LV}}{\partial \log c} \right)_T \quad (13)$$

and the equation is further simplified by taking the differential close to the CMC, at which point the linear nature of the EST renders the terms into the slope for a plot of surface tension against log C. Solving this equation at the CMC gives a surface excess of 2.93×10^{-10} mol/cm². The area per molecule may simply be considered another manner in which this behavior may be viewed and is determined in molecules per nm² from the relation:⁶

$$a_m^s = \frac{10^{14}}{N_{AV}\Gamma_m} \quad (14)$$

With N_{AV} being Avogadro's Number and Γ being expressed mol/cm². In this way a_m^s is determined to be 0.566 molecules per nm². These values are again seen to be in reasonable agreement with values for similar materials reported in the literature.

The calculated values from the above relationships are summarized in Table 4 along with the values for all salt solutions examined and literature values for similar surfactants located in literature sources.^{6,16}

Table 4. Surface Concentration and Occupied Area for C9-7EO

Solution	pH	Surface Concentration (Γ_m)		Occupied Area (a_m^s)	
		mol/cm ² (*10 ¹⁰)	Error (*10 ¹⁰)	molecule/nm ²	Error
Water	7.0	2.93	0.091	0.566	0.018
0.5M NaCl	6.9	1.41	0.075	1.18	0.066
0.5M KI	6.9	1.73	0.34	0.958	0.23
0.5M MgSO4	6.2	1.44	0.011	1.16	0.0088
0.5M Na ₂ SO4	6.8	1.97	0.040	0.844	0.018
0.5M CaCl ₂	6.4	2.33	0.25	0.711	0.085
0.5M CaCl ₂	4.1	1.71	0.28	0.971	0.19
0.5M CaCl ₂	9.7	1.82	0.28	0.912	0.16
0.5M CaCl ₂	10.3	2.13	0.28	0.781	0.12

4.3 FREE ENERGIES

The free energy of adsorption may be determined from the following equation:⁶

$$\Delta G_{ad}^0 = RT \ln a_\pi - \frac{\pi m}{\Gamma_m} \quad (15)$$

In which a_π is the activity of the surfactant in the aqueous phase at a surface pressure of π_m (that is, $\gamma_0 - \gamma_m$). In other words, π_m is the reduction of surface tension that occurs from a concentration of 0.00 M (the surface tension of pure water) to the CMC. It may be noted that the total expression for free energy of surface adsorption only has one term relating to the surface density of the surfactant itself; the first term is the overall free energy of aggregation on the part of the surfactant, also known as the free energy of micellization (i.e. $\Delta G_m^0 = RT \ln a_\pi$).¹⁵

For dilute systems of nonionic surfactants, mole fraction may be substituted for the activity term and the equation now becomes:⁶

$$\Delta G_{ad}^0 = RT \ln(CMC/\omega) - \frac{\pi_m}{\Gamma_m} \quad (16)$$

when ω is the number of moles of water in a liter (55.35 at 25° C). In this way it may be determined that for an aqueous solution of C9-7EO, the free energies of surface adsorption and micellization are -40.6 and -25.8 kJ/mol, respectively. These values are again typical of such surfactant systems and the values themselves make sense in light of typical behavior; the negative free energies indicate that the processes are spontaneous and the more negative ΔG_{ad} indicates that surface adsorption is preferred over micellization.¹

Table 5. Free Energies of Association for C9-7EO

Solution	pH	Free Energy of Adsorption (ΔG_{ad}^0)		Free Energy of Micellization (ΔG_m^0)	
		kJ/mol	Uncertainty	kJ/mol	Uncertainty
Water	7.0	-40.1	0.60	-25.3	0.13
0.5M NaCl	6.9	-58.6	1.8	-27.9	0.11
0.5M KI	6.9	-51.9	6.3	-26.7	0.10
0.5M MgSO4	6.2	-58.1	0.44	-27.7	0.21
0.5M Na ₂ SO4	6.8	-51.8	0.59	-29.8	0.13
0.5M CaCl ₂	6.4	-46.1	2.4	-27.2	0.10
0.5M CaCl ₂	4.1	-53.0	5.1	-27.4	0.10
0.5M CaCl ₂	9.7	-52.7	4.4	-27.6	0.11
0.5M CaCl ₂	10.3	-47.9	3.2	-27.3	0.10

4.4 DIFFUSION TO A NEW INTERFACE

Although equilibrium surface tension provides a wealth of information regarding the static effects of surfactants at an interface, a perturbation is required to infer kinetic information.¹⁹ The maximum bubble pressure technique provides this information by providing a dynamic surface which responds to applied surface pressure. The act of expanding a bubble produces a “new surface” that has less surfactant than a saturated surface and the rate at which the surfactant moves to the new surface is indicated by the measured surface tension upon variance of the surface age (see Figure 3 for an illustration).⁷

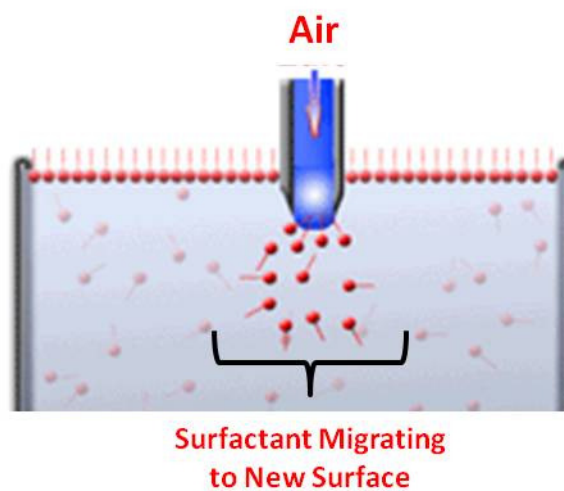


Figure 3. Illustration of a Maximum Bubble Pressure Dynamic Tensiometer

This effect may also be described as dilatation, or the expansion of a surface, which is assigned the parameter θ ($0.5 \cdot t^{-1}$, in which t is the age of the surface being expanded at a constant rate). A maximum bubble pressure tensiometer is particularly well suited in providing dilatation because by varying the volumetric flow of gas through the capillary orifice the dilatation and, by extension, the surface age may be similarly varied. Larger dilatations (smaller surface ages) emphasize diffusive effects as these dominate fast processes and smaller dilatations can allow determination of variances in slower

processes.¹⁸ The data produced in this manner for C9-7EO in a pre-micellar aqueous solution is shown in Chart 9.

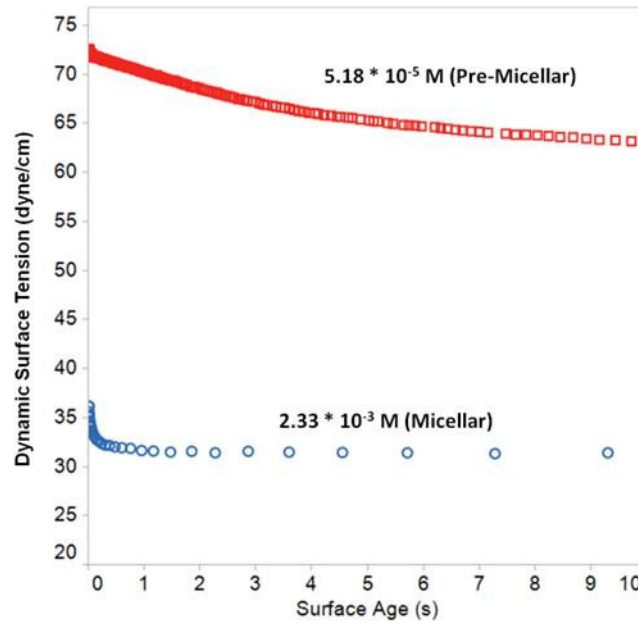


Chart 9. Dynamic Surface Tension of C9-7EO in Water as a Function of Surface Age

As previously described, the Ward-Tordai equation may be used to determine D_d with the simplifying assumption that bulk and subsurface concentrations are equal. If this condition is met, the equation becomes:

$$\gamma_{t \rightarrow 0} = \gamma_0 - 2RTC_0 \sqrt{\frac{D_d t}{\pi}} \quad (3)$$

Assigning $\gamma_0 - \gamma_t$ the term $\Delta\gamma_0$ and solving for that term leads to:

$$\Delta\gamma_0 = \left(\frac{D_d t}{\pi}\right)^{\frac{1}{2}} * 2RTC_0 \quad (17)$$

Squaring the entire equation and combining all terms held constant during the DST measurement into a single term, K, results in an equation approximating a linear form:

$$K\Delta\gamma_0^2 = D_d * t ; K = \frac{\pi}{(2RTC_0)^2} \quad (18)$$

In this way a linear regression may be employed in the case of $K\Delta\gamma^2$ vs. t in order to determine the diffusion coefficient, an illustration of which is provided in Chart 10. It may be seen that at further extensions of the surface age, the roughly estimated line ceases to describe the behavior of the solution. A simple explanation is that the assumptions behind equation (3) require an adherence to very short surface ages.²⁴

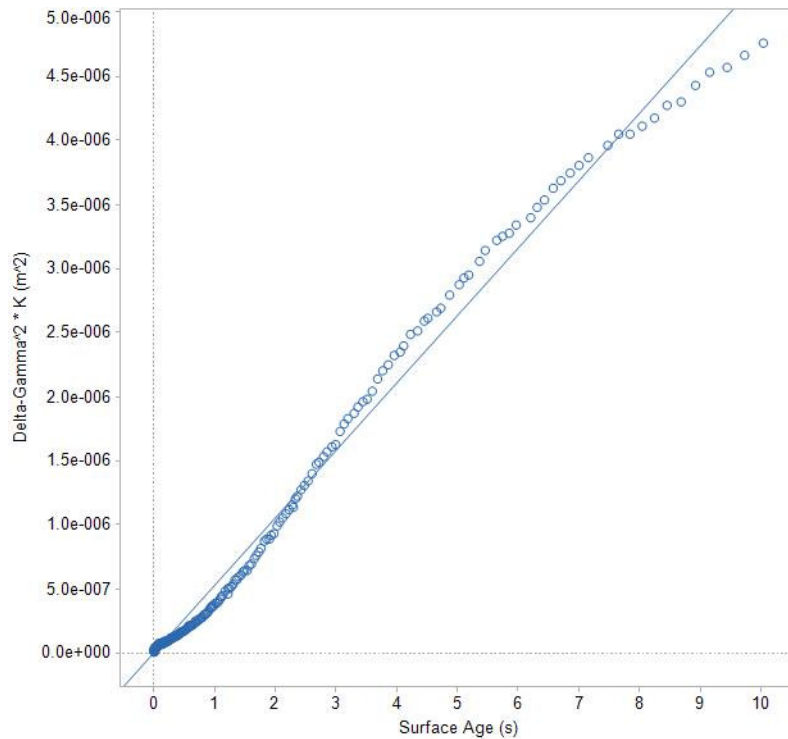


Chart 10. Plot of Linear Dynamic Surface Tension Variance as a Function of Surface Age

To begin the regression, data encompassing a surface age greater than 5 seconds was arbitrarily excluded. Although the correlation coefficient was reasonable (for the high throughput method of data acquisition), the error was enormous (see Table 6).

Furthermore, examination of the residuals plot (Chart 11) shows that there was a problem. Even 5 seconds was too old a surface age and this impression was enhanced by examination of the prediction plot (Chart 12), which showed a gradual loss of confidence as the surface age increased.

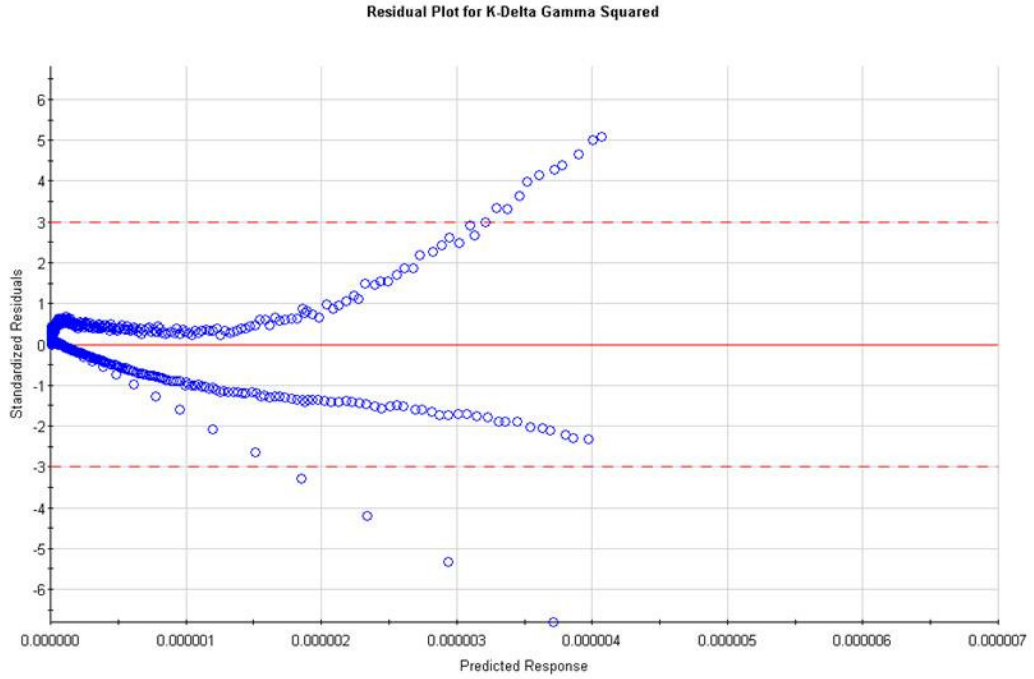


Chart 11. Residuals Plot for C9-7EO Regression for Diffusion Coefficient (Surface Age < 5 Seconds)

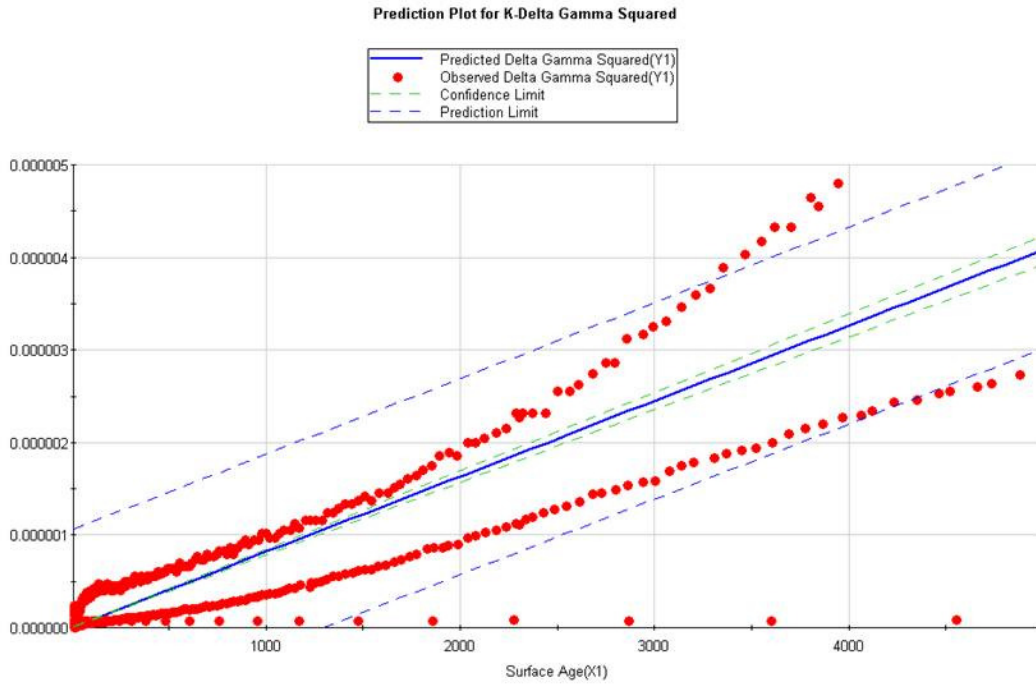


Chart 12. Prediction Plot for C9-7EO Regression for Diffusion Coefficient (Surface Age < 5 Seconds)

Examination of Charts 11 and 12 reveals a cluster of data that appears to maintain a relatively linear relationship at the shortest surface ages. The impact of diffusion should be essentially independent of concentration and this is validated by coincidental regression lines at that very small surface age.¹⁴

The benefit of massive data acquisition is that focusing on such a small point within the results still yields a respectable number of data points upon which to build a confident regression.²² Maximizing the surface age at 25 ms produced a lower correlation coefficient but a much lower RMSE and more randomly distributed residuals. Incrementally adding more data increased the correlation, but it also increased the error after a surface age of 30 ms. Examination of the residuals plot for a maximum of 40 ms (not shown) showed the trending of a pattern to the lower right, indicating that cohesion of a linear relationship was being lost. The coefficient of $1.23 \times 10^{-9} \text{ m}^2/\text{s}$ is thus accepted for this surfactant solution (see Table 6).

Table 6. Estimated Models for Determining the Diffusion Coefficient of C9-7EO in Water

Max Surface Age (ms)	Relative Error (RMSE)*10 ¹⁰	Correlation (R ²)	Significance (p)	D _d *10 ¹⁰ (m ² /s)
5000	5380	0.7500	<0.0001	8.16
25	26.9	0.8468	<0.0001	12.5
30	22.0	0.9102	<0.0001	12.3
40	29.5	0.9206	<0.0001	11.5

Via a similar method, diffusion coefficients were found for other solutions of C9-7EO and these are shown in Table 8, below.

4.5 ADSORPTION AT THE INTERFACE

Taking a similar approach as that described above for the determination of the adsorption coefficient, equation (4), leads to the following:

$$\frac{K}{(\gamma_t - \gamma_{eq})^2} = \frac{K}{\Delta\gamma_{eq}^2} = D_a t ; K = \frac{1}{\pi} * \left(\frac{RT\Gamma_{eq}^2}{C_0} \right)^2 \quad (19)$$

In this case the relationship held as the DST approached the EST (i.e., the surface tension at the equilibrium point for that concentration) and so the arbitrary surface age at which the regression began at was 6 seconds. Initial examination of the results indicated a good model, but, again, the residuals plot showed that the model was not suitable (Chart 13). The pattern clearly indicated a quadratic model and quickly recasting the model validated that impression.

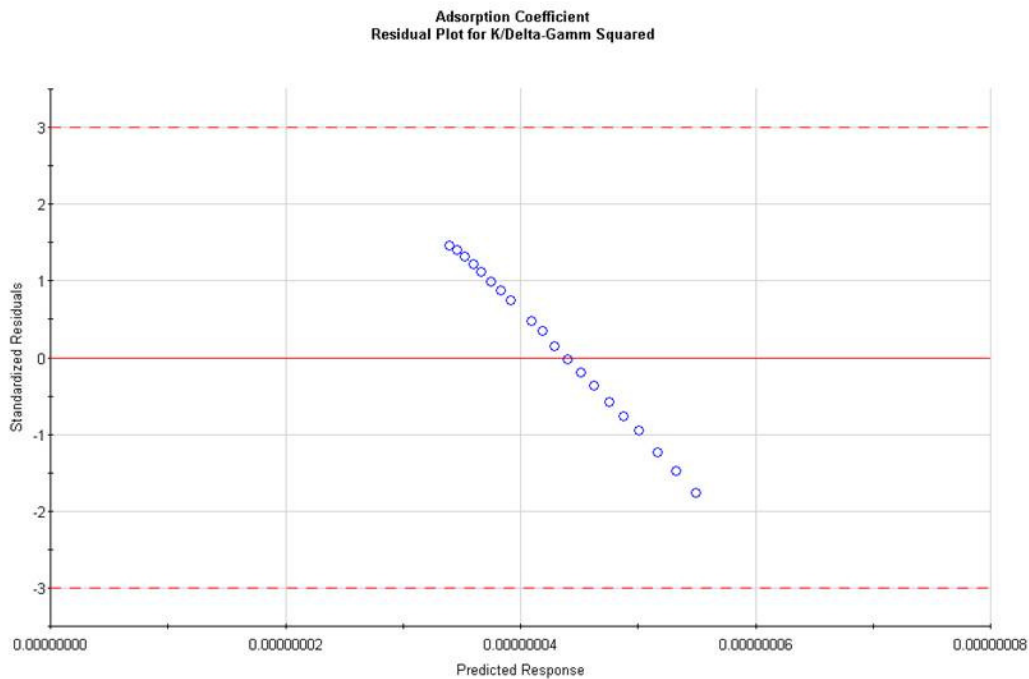


Chart 13. Residuals Plot for C9-7EO Regression for Adsorption Coefficient (Surface Age > 6 Seconds)

Of course, a quadratic model is dependent upon two variables rather than one and a “cross term” is due to the diffusion and adsorption coefficients both being involved.^{22,23} Furthermore, although the diffusion should be independent of concentration, the adsorption coefficient will not be independent of that variance until the CMC is met due to the increasing surface concentration that leads to more and more crowding at the interface.¹⁵ The manner in which to address this would therefore be to use a single concentration at the CMC so that the aforementioned micellar effects can be discounted but the impact of the adsorption coefficient would be maximized.

Additionally, the data to be examined would be at the longest possible surface ages without attaining equilibrium. Ideally the diffusion process would come to equilibrium relatively quickly so that the subsurface concentration of surfactant would be the same as the bulk concentration, but adsorptive effects would still be in process so that those final effects could be observed with little interference.

Extending data acquisition to a surface age between 9 and 20 seconds resulted in a nearly linear relationship, as indicated by the residuals plot. The statistics of the model are shown in Table 7. In this case the best model is shown by the second, including data points older than 10 seconds in terms of surface age. As more or less points were excluded, error increased significantly and, in the case of surface age greater than 11 seconds, model confidence was lost as well. An apparent diffusion coefficient was thus calculated to be $2.64 \times 10^{-12} \text{ m}^2/\text{s}$.

Table 7. Estimated Models for Determining the Apparent Diffusion Coefficient at CMC.

Min Surface Age (s)	Relative Error (RMSE)* 10^{10}	Correlation (R^2)	Significance (p)	$D_a \cdot 10^{12}$ (m^2/s)
9	13.5	0.9833	<0.0001	2.89
10	9.27	0.9889	<0.0001	2.64
11	7.41	0.9909	0.0015	2.52

With the adsorption coefficient in hand a determination regarding the energy cost of adsorbing at the interface may be determined by using equation (5):

$$D_a = D_d * \exp\left(-\frac{2E_a}{kT}\right) \quad (5)$$

In this way the energy of adsorption was determined to be ~8 kJ/mol. The same method is employed to determine the range of E_a for the other solutions of C9-7EO and this information is shown in Table 8.

Table 8. Coefficients of Diffusion and Adsorption with Energy of Adsorption

Solution	pH	Diff. Coefficient (D_d)		Ads. Coefficient (D_a)		Energy of Ads. (E_a)
		(m^2/s)* 10^9	Error* 10^9	(m^2/s)* 10^{12}	Error* 10^{12}	(kJ/mol)
Water	7.0	1.23	2.20	2.64	92.7	7.62
0.5M NaCl	6.9	5.30	11.7	6.78	14.8	8.26
0.5M KI	6.9	1.86	7.13	9.19	25.9	6.58
0.5M MgSO4	6.2	0.446	6.78	1.46	22.9	7.09
0.5M Na ₂ SO4	6.8	0.520	3.49	2.55	3.80	6.59
0.5M CaCl ₂	6.4	0.635	4.77	16.4	23.4	4.53
0.5M CaCl ₂	4.1	0.545	6.13	3.57	85.4	6.23
0.5M CaCl ₂	9.7	1.18	7.22	5.91	17.4	6.57
0.5M CaCl ₂	10.3	0.302	3.27	6.00	13.8	4.86

Error for the above coefficients is quite high and is an artifact of the high throughput methodology. Although the accuracy is excellent, the precision is lost in favor speed and in this situation the additive error ended any degree of confidence in precise calculations.

4.6 RATE OF DEMICELLIZATION

The final step in establishing potential effects of electrolytes on movement of detergent grade surfactant monomers to an interface in a cleaning process was to determine the rate of demicellization. As noted, equation (4) may be used to describe the reduction of surface tension as a function of time above the CMC via utilization of the apparent diffusion coefficient. By stating that micelles are not surface active and that the barrier to adsorption is similar above and below the CMC, equation (4) was enhanced by Rillaerts and Joos:¹⁸

$$\gamma_{t \rightarrow \infty} = \gamma_{eq} + \frac{RT\Gamma_m^2}{2C_0t} \sqrt{\frac{1}{D_a k}} \quad (6)$$

The new variable, k, is the rate of demicellization. This equation could be solved in the same manner as above, but obtaining linearity through this method is not possible with the experimental methods employed in this study. As a result consideration shifted to the

use of dilatation combined with the diffusion coefficient to describe a variable that prevents restoration of concentration to the subsurface layer. In this way equation (7) is used:

$$\gamma_{t \rightarrow 0} = \gamma_0 - \Gamma_{eq} \frac{d\gamma}{d\delta} * \frac{\theta}{(Dk)^{\frac{1}{2}}} \quad (7)$$

Simplification of this equation is easily done, and the final equation to be solved is:

$$\Delta\gamma_0^2 = \left(\frac{\gamma_t}{\pi}\right)^2 \frac{1}{t} * \frac{1}{k} \quad (20)$$

The demicellization constant will vary with concentration (greater concentration lead to a lower apparent demicellization rate due to a number of factors discussed below) so grouping of data points is not possible.^{18,14} Chart 14 shows four concentrations and their associated regression lines and the numerical values are shown in Table 9. A common method in reporting the demicellization rate is also to report the concentration as a multiple of CMC and this is convention is maintained in Tables 9 and 10, Table 10 being the completed listing of all solutions tested for this study.

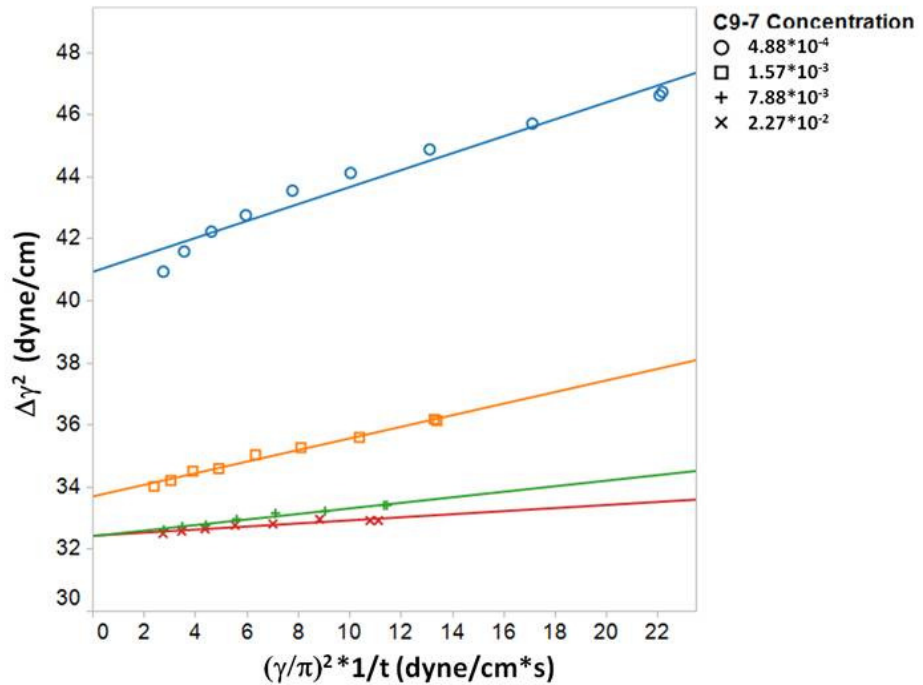


Chart 14. Graphical Determination of Demicellization Constant

Table 9. Demicellization Rate Constants for Aqueous Concentrations of C9-7EO.

Concentration (M)	*CMC	Relative Error (RMSE)	Correlation (R^2)	Significance (p)	k (s^{-1})
$4.88 \cdot 10^{-4}$	0.24	0.427	0.9615	<0.0001	1.57
$1.57 \cdot 10^{-3}$	0.79	0.0925	0.9882	<0.0001	2.70
$7.88 \cdot 10^{-3}$	3.9	0.0519	0.9758	<0.0001	5.88
$2.27 \cdot 10^{-2}$	11	0.0638	0.8815	0.0005	7.14

The error are reported in Table 10 is significantly lower than previously calculated coefficients and one might immediately question why it is as low as reported. Clever mathematics on the part of Rillaerts and Joos is responsible for this apparent disconnect. In the process of substituting the term describing the bubble dilatation, Dd cancelled out. More than simple hand waving, this effect is possible because of the high bulk concentration and older surfaces that were examined. A skeptical reader is encouraged to refer to the referenced article to examine the nuances of an interesting trick that plays out very well in analysis.

Comparing demicellization rates for other nonionic surfactants in aqueous solutions, there is a great deal of similarity both in trending and in magnitude, although no studies have been found that are significantly close to the C9-7EO in size and structure.^{14,13,18}

Table 10. Demicellization Rate Constants for All Tested Solutions of C9-7EO.

Salt	pH	Concentration (M)	*CMC	k(s ⁻¹)	Error
None	7	4.88*10 ⁻⁴	0.24	1.57	0.43
		1.57*10 ⁻³	0.79	2.70	0.09
		7.88*10 ⁻³	3.9	5.88	0.05
		2.27*10 ⁻²	11	7.14	0.06
NaCl	6.9	1.33*10 ⁻³	2.2	2.28	0.77
		4.32*10 ⁻³	7.2	2.73	0.18
		1.48*10 ⁻²	24	5.84	0.092
		2.58*10 ⁻²	43	8.13	0.093
KI	6.9	1.77*10 ⁻³	2.0	1.92	2.45
MgSO4	6.2	1.54*10 ⁻³	2.4	1.69	0.51
		4.19*10 ⁻³	6.5	2.42	0.22
		1.39*10 ⁻²	21	6.80	0.12
		2.20*10 ⁻²	34	8.77	0.1
Na2SO4	6.8	5.77*10 ⁻⁴	2.0	0.192	1.9
		1.73*10 ⁻³	6.2	0.282	0.3
		7.45*10 ⁻³	26	2.92	0.11
		2.54*10 ⁻²	90	5.56	1.2
CaCl2	6.4	1.36*10 ⁻³	1.8	2.56	0.53
		3.50*10 ⁻³	4.5	2.89	0.28
		1.20*10 ⁻²	16	4.20	0.15
		2.06*10 ⁻²	27	5.29	0.23
	4.1	2.68*10 ⁻³	3.7	2.94	0.22
		5.44*10 ⁻³	7.5	4.74	0.1
		1.41*10 ⁻²	20	6.99	0.12
		3.16*10 ⁻²	44	8.33	0.08
	9.7	8.24*10 ⁻⁴	1.2	2.26	0.79
		2.36*10 ⁻³	3.5	2.62	0.31
		7.14*10 ⁻³	11	5.59	0.13
		2.49*10 ⁻²	37	8.62	0.091
	10.3	5.34*10 ⁻⁴	0.71	2.12	0.53
		2.14*10 ⁻³	2.8	2.85	0.27
		4.26*10 ⁻³	5.6	4.61	0.14
		2.64*10 ⁻²	35	10.2	0.067

CHAPTER 5

DISCUSSION OF RESULTS

The particular salt solutions were chosen to provide variance in terms of solution ionic strength and ion size. The anticipation was that the discussion would be guided by the apparent impact of the solution properties. The properties of the salt solutions are given in Table 11 to guide further commentary.

Table 11. Solution and Ion Properties of Base Solutions.

Solution	M	(-) ^a	(+) ^a	(-) Size ^b	(+) Size ^b	Average Size ^b	Ionic Strength ^c	pH
Water	0	0	0	0	0	0	0	7
NaCl	0.5	1	1	167	116	142	0.5	6.9
KI	0.5	1	1	206	152	179	0.5	6.9
MgSO ₄	0.5	2	2	308	86	197	2	6.2
CaCl ₂	0.5	1	2	167	114	132	1.25	6.4
Na ₂ SO ₄	0.5	2	1	308	116	244	1.25	6.8
CaCl ₂ /HCl	0.5	1	2	167	114	132	1.25	4.1
CaCl ₂ /Ca(OH) ₂	0.5	1	2	167	114	132	1.25	9.7
CaCl ₂ /Ca(OH) ₂	0.5	1	2	167	114	132	1.25	10.3

^a Valence of anion/cation

^b Size given in picometers²⁵

^c Ionic strength given by standard calculation ($I = \sum c_i z_i^2$)²⁶

The first point to note is that the equilibrium surface tension is nearly identical across all solutions. The general trend indicates that the EST may actually be lowered via the addition of salt (and some of the difference is right at the edge of propagated error, so there may indeed be some significance), but the first look indicates that surface aggregation at equilibrium is independent of salt presence. This is to be expected for a nonionic surfactant, so it is not particularly surprising.

It has been established that the addition of a salt to a surfactant solution will decrease the CMC.^{6,1,5} The surprising point in the case of C9-7EO is that there may be a variance in the degree of depression. Comparing two monovalent salts (KI and NaCl), one sees that the NaCl depresses the CMC further. The first consideration to come to mind is the

effective hydration radius of the ions. By indirect interaction with the hydrophobe through the hydration radius of the ion, the salt solution is effectively dehydrating the environment of the surfactant and making the surfactant more “hydrophobic” in the given solution.⁶ This is a reflection of real effects seen in changing the hydrophilic-lipophilic balance (HLB), so this is again a good reflection of known, real world effects. The effect of the hydration radius is far reaching as one sees that two of the lowest CMC’s result from the use of a sulfate anion, which is considerably larger than any of the other ions when taken with the propagated error. Furthermore, in the case of the KI and NaCl salts, the larger ions may result in a more diffuse effect regarding the interaction with water such that NaCl has a more noticeable impact.

Another interesting effect to note is that pH changes have no impact on the CMC within the distribution. Again, this is not particularly surprising, but many detergent formulators often embrace simple alkalinity (provided by NaOH or KOH) as an effective way to build performance of a surfactant based system.^{3,2,4} It is seen here that the presence of the counterions has more impact on the surfactant performance than the hydroxyl ion.

If one considers the presence of ions as particles affecting the solvent rather than the surfactant such as indicated above through the discussion of hydration radius and the resulting impact on the hydrophobe, then perhaps a better approach is to consider ions as particles. In this way ionic strength no longer has as much sway in terms of solvent interaction but the actual number of dissociated particles does. This different viewpoint is illustrated in Table 12. Consider each ion as a particle with no consideration being given to valence, but to actual size. Rather than calculating a hydration radius, the electron radius will be used as a quick examination tool. A weighted average was also taken as a simple way to extend size effects throughout the entire concentration, and the number of particles was also multiplied by the average size. A thorough treatment of this idea would also include a consideration of polarizability on the part of the ions, but for the sake of brevity this will be examined in future work.

Table 12. Tabular Explanation of Anions and Cations as General Ionic Particles

Solution	M	Dissociated Particles	Moles of Particles	Average Size ^b	Particles *Size
Water	0	0	0	0	0
NaCl	0.5	2	1	142	142
KI	0.5	2	1	179	179
MgSO ₄	0.5	2	1	197	197
CaCl ₂	0.5	3	1.5	132	198
Na ₂ SO ₄	0.5	3	1.5	244	366
CaCl ₂ /HCl	0.5	3	1.5	132	198
CaCl ₂ /Ca(OH) ₂	0.5	3	1.5	132	198
CaCl ₂ /Ca(OH) ₂	0.5	3	1.5	132	198

Taking this approach and plotting the CMC against the number of particles times their average size actually shows a trend that had not been seen when examining the data in light of ionic strength, valence effect, or size alone (See Chart 15). Due to the limited data available, this is far from definitive, but the impact of dissolved salts is certainly in evidence, particularly when taken with the propagated error of the system (marked with arrows to show confidence level). A linear trendline has been added to guide the eye, but the effect could also be logarithmic in nature (in fact that appears more likely).

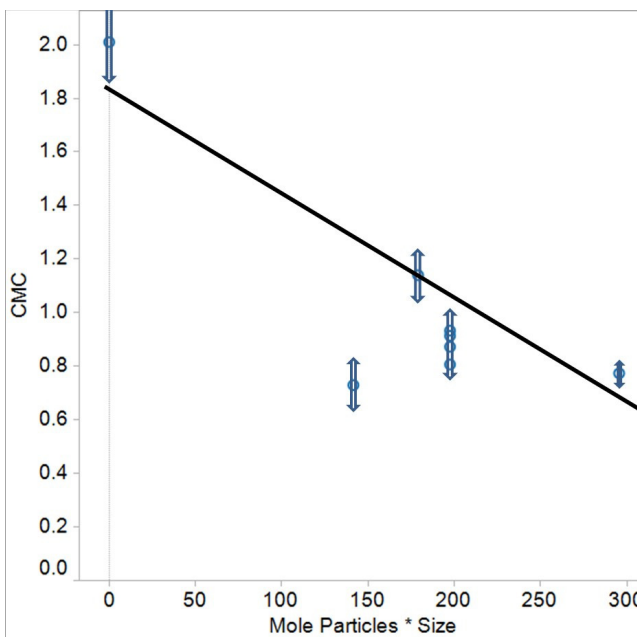


Chart 15. Critical Micelle Concentration as a Function of (Ionic Radius)*(Total M of Ions)

In considering the effect of surface concentration one might be tempted to consider the effect as a different aspect of the same behavior noted with the shifting CMC but a quick check to determine the normal relationship (plotting the CMC against Γ_m) turns up no obvious trend and suggests that surface concentration must be taken alone.

Unfortunately a hard correlation of any type is difficult to find. Within the error distribution extremes are represented across the spectrum and it would make more sense to experiment further with replicate sets. One thing that is noteworthy, however, is that Γ_m is decreased in every case. This is likely due to the hydration radius of the ions mentioned above in that there is now excluded surface area that the surfactant cannot adsorb to. On the other hand, the free energy of adsorption (ΔG_{ad}^0) drops significantly and contemplation of the effects at the surface (particularly the added self adhesion of water due to the loss of one dimension of interaction) provides a simple answer. A homogenous surface provides a homogenous surface energy, but adding ionic material shifts the topography on a molecular level. Orientation of water to hydrate ions produces stronger and weaker interactions, the latter of which produces less resistance to the hydrophobic tail of a surfactant as it orients itself at the surface.²⁷ Taking this concept back to the trend noted with the CMC provides further assurance that hydration radius and particle number is the key to most efficient surface effect.

On the other hand, the free energy of micellization (ΔG_m^0) remains unchanged by the presence of ions. Considering that the barrier to micellization is one of opportunity (the surfactant adsorbs preferentially at a surface prior to aggregating), this is not surprising. The entropic effect is the primary hurdle in micellization, so charged particles should have no effect.

In moving to examine the kinetic effects of the salt solutions it becomes clear that at the level of precision necessary, the high throughput methodology will not work to provide hard numbers and possibly not even good trending information in determining the diffusion and adsorption coefficients. Even with massive data sets the base error cannot be transcended. Rather than having hard numbers with an error distribution the data

devolves into probabilities with spreads which are all-encompassing of the systems examined. Nonetheless one remains hopeful that the trends seen may provide some guidance and will be examined for an indication of future direction.

Considering that C9-7EO is a nonionic surfactant, it certainly makes sense that the adsorption coefficient (D_a) is significantly lower than the diffusion coefficient (D_d). Beyond crowding and orientation there is little in the way of a significant energy barrier to prevent adsorption. Additionally, there is little that may be said regarding an adjustment to the diffusion coefficient due to the significant degree of uncertainty. Looking at the general trend, however, it appears that the rate of diffusion is lessened by the addition of electrolytes. This may again go back to the idea of large particles with hydrated radii, in that such particles may provide a barrier to the random walk of diffusion. The impact is minimal if it is present at all.

The rate of demicellization is more firm, however, particularly at the higher concentrations. Consideration of all data obtained and examined to this point would seem to indicate that micellization/demicellization effects of salts would not be noted. However, if one considers the micelle aggregate as an “interface in miniature,” then the effects at play at the interface will be similarly active at the point of demicellization. Just as the surfactant monomer is moved to the interface, the micelle may be stabilized, and it appears that this is exactly what is happening as evidenced in Chart 16. In this chart it may be seen that the fastest measured rate of demicellization occurs when there is nothing but water and surfactant in solution. All salts have a slower rate with the slowest by far being sodium sulfate, which is also the surfactant with the highest size*particle number score.

By way of further guidance in interpreting Chart 16, note that the size of the “bubbles” are in correlation with the size*number of particles and that the trend from smallest (or none in the case of no salt) to largest bubbles moves from the lower right to the upper left. The trend lines are present to help guide the eye and are not representative of any meaningful regression.

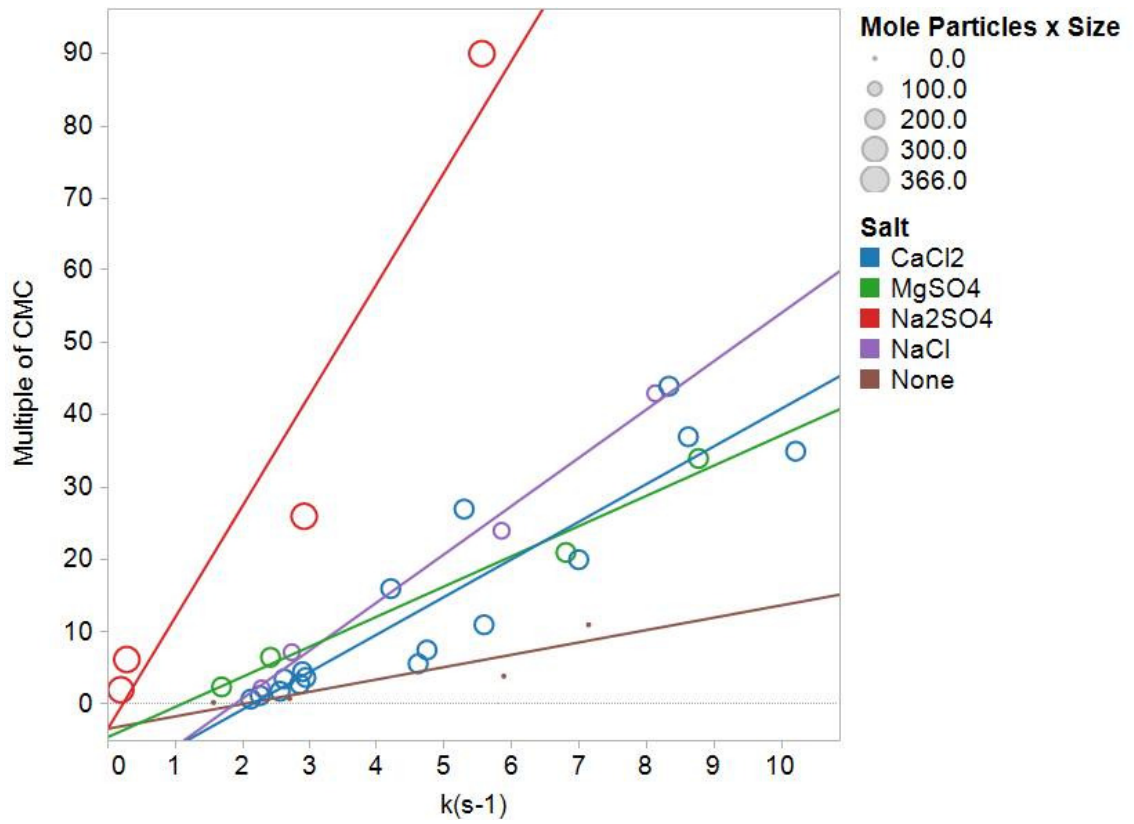


Chart 16. Rate of Demicellization Constant as a Function of Concentration

CHAPTER 6

CONCLUSION

In this study the critical micelle concentration, equilibrium surface tension, and excess surface concentration for C9-7EO was determined for both simple aqueous solutions and for a variety of salt solutions at 0.5 M in concentration. Further details were examined in terms of thermodynamic and kinetic effects and some interesting behavior was seen. More importantly, an understanding has begun to develop regarding the interaction of salts with this particular surfactant.

Salt composition does indeed impact the behavior of the surfactant micelles as evidenced by the rate of demicellization measured via maximum bubble pressure tensiometer. The primary factors involved are the radius of ions and the number of dissociated particles. This is not to say that ionic strength is an indicator of the observed effects, as this particular measure shows poor correlation with the changes noted in varied solutions, rather a simpler calculation of number of particles multiplied by the electronic radius correlates effects more clearly for a nonionic surfactant system.

In terms of effective utilization of these noted trends there is likely a balance to be struck between the slower demicellization rate and the more active interface, both of which will result from a higher score of particle number**size*. Unfortunately the high throughput methodology was not able to produce distinctions as fine as necessary to say unequivocally that the issue is diffusive, although indicators certainly point that way.

In terms of moving forward, there are two directions to take. The first is to continue the development of a good understanding of the molecular processes involved. This path would begin by making a series of dilutions conforming to a tight specification for testing at low surface ages to minimize error in the value of the estimated diffusion coefficient (D_d) for different salt types. This process is of interest because adsorption for nonionics is primarily diffusion controlled and if the micellar impact is to be understood, then the adsorption rate must accurately be quantified. The second step will be to make stepwise

concentrations in two dimensions, that of the surfactant concentration and that of the salt concentration to be evaluated at slow dilatations so that a coefficient may be assigned to the rate of demicellization.

The other path, which may be taken at the same time, moves to other salts, specifically those that are more common within cleaning products. One of the goals was to establish that surface interaction is independent of pH and, having shown that it is, the next step is to examine more closely the typical builder salts with confidence that pH effects may be discounted. In this way one may be able to eventually evaluate formulas containing materials such as sodium metasilicate and sodium carbonate to assess an optimal surfactant load in terms of efficiency and cost effectiveness.

The final goal in this process is not so much to determine a so called “optimum” in developing a concept of surfactant behavior in the presence of ionic builders, but to provide an understanding. Each application area brings a different set of circumstances with a different optimal solution in terms of detergent behavior and by balancing the idea of adsorption kinetics with micellization kinetics an optimum may be available on a single, specific application basis.

Although further study might be interesting in the area of actual relaxation rates, this is likely unnecessary for the purposes of the goal unless it is pursued to simplify the determination of adsorption. Of greater interest however, is how the free energy of demicellization is impacted. The free energy of micellization does not change due to salt effects, as expected, but there is a stabilizing effect from the salt concentration and the exploration of the detailed interactions behind this effect for the surfactant at hand would be invaluable in using the material in specific applications.

REFERENCES

-
- ¹ Danahayake, Manilal, and Milton J. Rosen. *Industrial Utilization of Surfactants: Principles and Practice*. Chicago: AOCS Press, 2000.
- ² Urban, David G. *How to Formulate and Compound Industrial Detergents*. Lexington: David G. Urban, 2002.
- ³ Flick, Ernest W. *Advanced Cleaning Product Formulations*. Park Ridge: Noyes Publications, 1995.
- ⁴ Milwidsky, B.M. *Detergent Analysis*. New York: John Wiley & Sons, Inc., 1982.
- ⁵ Lange, K. Robert. *Surfactants: A Practical Handbook*. Cincinnati: Hanser Gardner Publications, Inc., 1999.
- ⁶ Rosen, Milton J. *Surfactants and Interfacial Phenomena (2nd Ed.)*. New York: John Wiley & Sons, Inc., 1989.
- ⁷ Patist, A., B.K. Jha, S.G. Oh, and D.O. Shah. "Importance of Micellar Relaxation Time on Detergent Properties." *Journal of Surfactants and Detergents*, 1999: 317-324.
- ⁸ Shell Chemical Company. *Neodol Ethoxylates and Competitive Nonionics Properties Guide*. Industrial Surfactant Properties Compilation, Houston: Shell Chemical Company, 1994.
- ⁹ For an example simply look to Reference #20, which is Volume 72 of the Surfactant Science Series.
- ¹⁰ Danov, K.D., P.A. Kralchevsky, N.D. Denkov, K.P. Ananthapadmanabhan, and Alex Lips. "Mass Transport in Micellar Surfactant Solutions: 2. Theoretical Modeling of Adsorption at a Quiescent Interface." *Advances in Colloid and Interface Science*, 2006: 17-33.
- ¹¹ Landazuri, G., et al. "Aggregation and Adsorption Behavior of Low Concentration Aqueous Solutions of Hexadecyltrimethylammonium ortho-, meta-, and para-Fluorobenzoate." *Journal of Colloid and Interface Science*, 2012: 86-93.
- ¹² Patist, A., S.G. Oh, R. Leung, and D.O. Shah. "Kinetics of Micellization: Its Significance to Technological Processes." *Colloids and Surfaces*, 2001: 3-16.
- ¹³ Danov, K.D., P.A. Kralchevsky, N.D. Denkov, K.P. Ananthapadmanabhan, and Alex Lips. "Mass Transport in Micellar Surfactant Solutions: 1. Relaxation of Micelle Concentration, Aggregation Number, and Polydispersity." *Advances in Colloid and Interface Science*, 2006: 1-16.
- ¹⁴ Kjellin, U.R. Mikael, Johan Reimer, and Per Hansson. "An Investigation of Dynamic Surface Tension, Critical Micelle Concentration, and Aggregation Number of Three Nonionic Surfactants Using NMR, Time-Resolved Fluorescent Quenching, and Maximum Bubble Pressure Tensiometry." *Journal of Colloid and Interface Science*, 2003: 506-515.
- ¹⁵ Yoshimura, Tomokazu, Kanae Nyuta, and Kunio Esumi. "Zwitterionic Heterogemini Surfactants Containing Ammonium and Carboxylate Headgroups. 1. Adsorption and Micellization." *Langmuir*, 2005: 2682-2688.
- ¹⁶ Azizian, Saeid, et al. "Analysis of Dynamic Surface Tension of Tetraethylene Glycol Monoethyl Ether at Air/Water Interface." *Colloid and Polymer Science*, 2007: 1699-1705.

-
- ¹⁷ Yoshimura, Tomakazu, Akiko Ohno, and Kunio Esumi. "Equilibrium and Dynamic Surface Tension Properties of Partially Fluorinated Quaternary Ammonium Salt Gemini Surfactants." *Langmuir*, 2006: 4643-4648.
- ¹⁸ Rillaerts, E., and P. Joos. "Rate of Demicellization from the Dynamic Surface Tensions of Micellar Solutions." *Journal of Physical Chemistry*, 1982: 3471-3478.
- ¹⁹ Christov, N.C., K.D. Danov, P.A. Kralchevsky, P. Kavssery, K.P. Ananthapadmanabhan, and Alex Lips. "Maximum Bubble Pressure Method: Universal Surface Age and Transport Mechanisms in Surfactant Solutions." *Langmuir*, 2006: 7528-7542.
- ²⁰ Os, Nico M. van. *Nonionic Surfactants: Organic Chemistry (Surfactant Science Series: Volume 72)*. Cleveland: CRC Press, 1998.
- ²¹ Schubert, K.V., R. Strey, and M. Kahlweit. "3PHEX: A New Surfactant Purification Technique." *Progress in Colloid and Polymer Science*, 1991: 103-106.
- ²² Beebe, Kenneth R., Randy J. Pell, and Mary Beth Seasholtz. *Chemometrics: A Practical Guide*. New York: John Wiley & Sons, Inc., 1998.
- ²³ Hill, T., and P. Lewicki. *Statistics: Methods and Applications*. Tulsa: StatSoft, 2007.
- ²⁴ Bhole, Nikhil S., Fenfen Huang, and Charles Malderelli. "Fluorescence Visualization and Modeling of a Micelle-Free Zone Formed at the Interface between adn Oils and an Aqueous Micellar Phase during Interfacial Surfactant Transport." *Langmuir*, 2010: 15761-15778.
- ²⁵ Wikipedia. Ionic Radius. http://en.wikipedia.org/wiki/Ionic_radius (accessed 2012).
- ²⁶ Harris, Daniel C. *Quantitative Chemical Analysis*, 8th Edition. New York: W.H. Freeman and Company, 2010.
- ²⁷ Pinazo, Aurora, Xinyun Wen, Lourdes Perez, Maria-Rosa Infante, and Elias I. Franses. "Aggregation Behavior in Water of Monomeric and Gemini Cationic Surfactants Drived from Argenine." *Langmuir*, 1999: 3134-3142.

ADDITIONAL REFERENCES

Danov, Krassimir D., Peter A. Kralchevsky, Nikolai D. Denkov, Kavssery P. Ananthpadmanabhan, and Alex Lips. "Dynamics of Adsorption from Micellar Surfactant Solutions at Expanding Fluid Interfaces in Relation to the Emulsification Process." Proceedings of the 4th World Congress on Emulsions. Lyon, 2006. 1-376.

Lin, Shi-Yow, Ya-Chi Lee, Ming-Jian Shao, and Ching-Tien Hsu. "A Study on Surfactant Adsorption Kinetics: The Role of the Data of Equation of State for C14E8." Journal of Colloid and Interface Science, 2001: 372-376.

Maeda, Hiroshi. "Thermodynamic Analysis of Micellar Systems." In Encyclopedia of Surface and Colloid Science, by P. Somasundaran, 6221-6233. Cleveland: CRC Press, 2006.

Sterling, Mary Jane. Linear Algebra for Dummies. Hoboken, NJ: Wiley Publishing, Inc., 2009.

APPENDIX A

STANDARDIZING THE JANUS FORMULATOR

The Janus formulator (shown in Picture A1) was built to aid in screening chemical properties and is thus ideal for the generation of large amounts of data.²⁸ A robotic arm incorporates eight pipettes which may be fitted with disposable tips. Each pipette has its own pump (Picture A2, top) and may provide “system liquid” from a reservoir or may aspirate material provided (“neat substance” or “neat material”), either of which is then delivered to selected receptacles, such as the tubes shown in Picture A2 (bottom).



Picture A 1. Janus Formulator (left) and Transfer Pumps (right)

The unit works from a volume rather than mass basis with no feedback to ensure that the requested amount is delivered. For this reason the actual error of each pipette/pump must be determined and, if possible, corrected or taken into account. The first step in utilizing the Janus for this study was quantification of the variances or error on the part of the pipettes, both for the system liquid (in this case water) and for the materials individually aspirated by the pipettes (provided by the experimenter and generally dilute surfactant or electrolyte solutions). Through some oversight the controlling computer program will

not allow the user to individually calibrate each of the pumps to fine tune delivery or dispensing. Adjustments may be made, but only in a manner that affects all eight tips, so an additional goal to be met is to determine which of the pipette tips are most similar in terms of error so that those may be used in concert to maximize the efficiency of the unit.



Picture A 2. Janus Formulator Components; Dispense Pumps (top) and Sample Tubes (bottom)

The greatest benefit of generating a large amount of data is that random variances become self-correcting because these variances cluster around a central mean which is the theoretically “correct” value. Variances of the amount of system liquid or material delivered by the Janus may or may not be truly random, however, and thus the mean might be skewed away from the correct value sought. The purpose of the following exercise is to determine and quantify non-random error to the greatest extent possible.²²

A.1 THE FIRST PASS

In the first round of testing, the Janus was instructed to dispense unit amounts of system liquid and neat material and the receiving containers were weighed on an analytical balance in between operations. A sample of the raw data resulting from this operation is shown in Table A1 (only a sample because the volume of data accumulated in this manner is quite large). In this table the System Tip and Neat Tip refer to the pipette tip specified for that sample, the Tare is the mass of the receptacle tube, the System and Neat Gross is the mass of the receptacle tube after the dispensing of the specified liquid, the System and Neat Net is the calculated mass of the liquid delivered in that step, System and Neat Disp. Is the volume of liquid dispensed (for ease of calculation, solutions with a specific gravity of 1.000 at 25° C were used for the calibration process through the incorporation of either NaCl or isopropanol as necessary), and the System and Neat Call is the volume of liquid which the control program called for at that step.

Table A1. Sample Data Points Taken During Standardization of the Janus Formulator.

Sample #	System Tip	Neat Tip	Tare(g)	System Gross(g)	System Net(g)	System Disp.(μ l)	System Call (μ l)	Neat Gross (g)	Neat Net (g)	Neat Disp. (μ l)	Neat Call (μ l)
7	7	1	11.5044	21.4887	9.9843	9984.3	9980	21.5086	0.0199	19.9	20
8	8	1	11.6907	21.6597	9.9690	9969.0	9980	21.6794	0.0197	19.7	20
9	1	1	11.5099	21.4840	9.9741	9974.1	9980	21.5038	0.0198	19.8	20
10	2	1	11.6841	21.6422	9.9581	9958.1	9970	21.6716	0.0294	29.4	30
11	3	1	11.6658	21.6185	9.9527	9952.7	9970	21.6479	0.0294	29.4	30
12	4	1	11.7656	21.7249	9.9593	9959.3	9970	21.7545	0.0296	29.6	30
13	5	1	11.7666	21.7037	9.9371	9937.1	9950	21.752	0.0483	48.3	50
14	6	1	11.6497	21.6020	9.9523	9952.3	9950	21.6504	0.0484	48.4	50
15	7	1	11.7437	21.7005	9.9568	9956.8	9950	21.749	0.0485	48.5	50
16	8	1	11.5284	21.4496	9.9212	9921.2	9930	21.5172	0.0676	67.6	70
17	1	1	11.5077	21.4325	9.9248	9924.8	9930	21.4999	0.0674	67.4	70
18	2	1	11.794	21.7129	9.9189	9918.9	9930	21.78	0.0671	67.1	70
19	3	1	11.7579	21.6208	9.8629	9862.9	9880	21.7361	0.1153	115.3	120
20	4	1	11.5887	21.4585	9.8698	9869.8	9880	21.5734	0.1149	114.9	120
22	6	1	11.3634	21.1960	9.8326	9832.6	9830	21.3585	0.1625	162.5	170

23	7	1	11.5888	21.4259	9.8371	9837.1	9830	21.5877	0.1618	161.8	170
24	8	1	11.5387	21.3597	9.8210	9821.0	9830	21.52	0.1603	160.3	170
25	1	2	11.6195	21.6024	9.9829	9982.9	9990	21.6113	0.0089	8.9	10
26	2	2	11.7093	21.6858	9.9765	9976.5	9990	21.6958	0.01	10	10
27	3	2	11.4639	21.4346	9.9707	9970.7	9990	21.445	0.0104	10.4	10
28	4	2	11.6327	21.6052	9.9725	9972.5	9985	21.6204	0.0152	15.2	15
29	5	2	11.7575	21.7278	9.9703	9970.3	9985	21.743	0.0152	15.2	15
30	6	2	11.597	21.5833	9.9863	9986.3	9985	21.5985	0.0152	15.2	15
31	7	2	11.6744	21.6599	9.9855	9985.5	9980	21.6802	0.0203	20.3	20
32	8	2	11.4513	21.4211	9.9698	9969.8	9980	21.4409	0.0198	19.8	20
33	1	2	11.6598	21.6342	9.9744	9974.4	9980	21.6542	0.02	20	20
34	2	2	11.6873	21.6458	9.9585	9958.5	9970	21.6751	0.0293	29.3	30
35	3	2	11.6966	21.6487	9.9521	9952.1	9970	21.6777	0.029	29	30
36	4	2	11.505	21.4642	9.9592	9959.2	9970	21.4932	0.029	29	30

Plotting the amount requested against the amount delivered and generating trend lines of the individual performance of pipette tips via linear regression results in Charts A1 left and right, the performance examination of the system liquid dispensed and the provided material dispensed, respectively. A number of things are immediately apparent, the first of which is that the system has the potential to maintain a high degree of precision, although there may be outliers that will wreck that precision. Also apparent is the fact that the regressed line for each pipette tip is indeed noticeably different. Finally, the obvious point is that something went significantly wrong with tip #5 when dispensing neat substance. Examination of the data indicates that a column of data may have been shifted during record keeping, but this may have been a fortunate accident in that this careful analysis also revealed that evaporation is also a variance. This variance appears to become significant if a series is allowed to remain uncovered for a period of time longer than what is required to prepare the dilutions. The simple solution was to seal the tubes immediately after sample preparation.

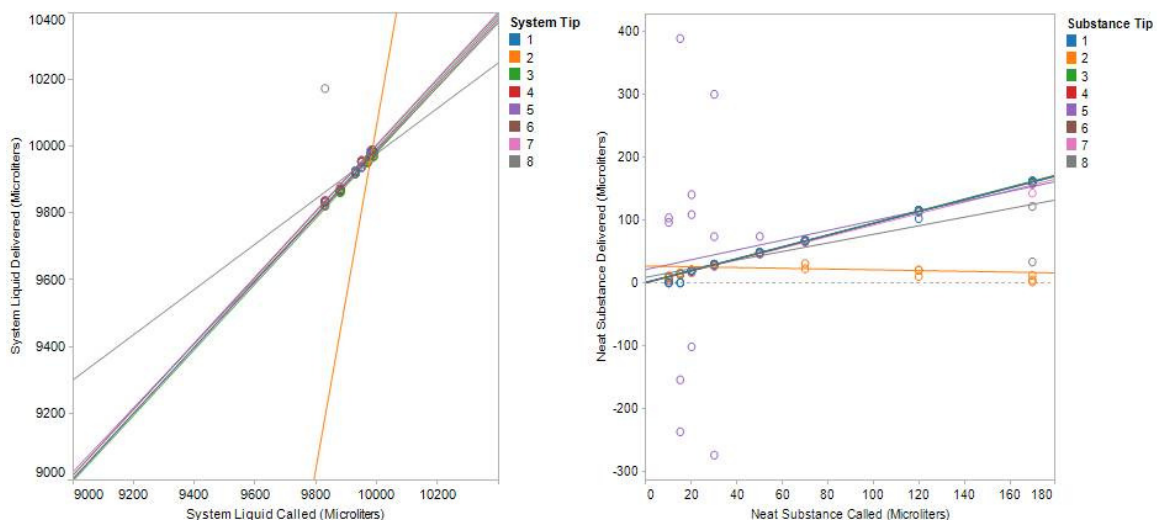


Chart A 1. Pipette Tip Performance and Trend Lines for System Liquid (left) and Neat Substance (right)

The obvious outliers that could not be anticipated or traced appear to be artifacts of the pumps and are generally due to air bubbles. One suitable approach to solving this problem was to use a dye marker to check for such gross outliers. This method is described in more detail in Appendix B, but the result is simply that such outliers are identified prior to acquisition of properties for a given dilution and discarded with confidence.

Once gross outliers are removed from the response two rather different sets of charts are developed. Pipette tip 4 is broken out individually in Chart A3 by way of illustration and Table A2 shows the slope and intercept (m and b, respectively) similarly developed for all eight tips in both dispensing modes.

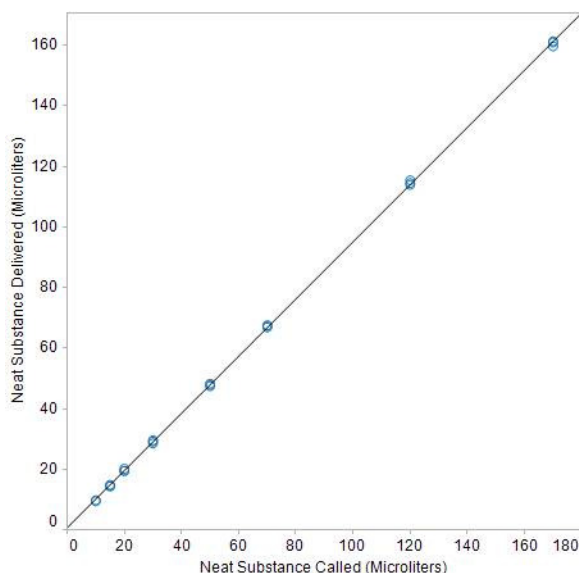


Chart A 2. Dispensing Performance of Pipette Tip#4 for Neat Substance After Outlier Exclusion

Table A2. Variances in Requested vs. Delivered Dosage of Material by Janus.

Tip #		Model: Delivered Dose = Requested*m + b (from $y = mx + b$)					
		Slope (m)	Intercept (b)	Correlation (R^2)	Standard Error (s)	Stat. Significance (p)	Relative Standard Error (RSE)
Neat Substance	1	0.9488	-0.2247	0.9999	0.5039	<0.0001	0.420%
	2	0.9405	-0.2780	0.9992	0.4836	<0.0001	0.403%
	3	0.9412	0.5084	0.9999	0.4299	<0.0001	0.358%
	4	0.9446	0.5207	0.9999	0.6199	<0.0001	0.517%
	5	0.9433	0.1441	0.9998	0.8348	<0.0001	0.696%
	6	0.9481	0.7414	0.9998	0.7671	<0.0001	0.639%
	7	0.9450	0.8095	0.9994	1.227	<0.0001	1.023%
	8	0.9454	-1.102	0.9996	0.8280	<0.0001	0.690%
	Overall:	0.9444	0.4035	0.9997	0.7576	<0.0001	0.631%
System Liquid	1	0.9929	65.12	0.9957	1.806	<0.0001	0.019%
	2	0.9444	542.2	0.9951	1.684	<0.0001	0.018%
	3	0.9856	124.8	0.9998	0.7607	<0.0001	0.008%
	4	0.9856	132.3	0.9998	0.6598	<0.0001	0.007%
	5	0.9616	369.8	0.9972	2.336	<0.0001	0.024%
	6	0.9899	104.4	0.9997	1.222	<0.0001	0.013%
	7	0.9921	85.25	0.9999	0.7945	<0.0001	0.008%
	8	0.9928	62.85	0.9996	1.183	<0.0001	0.012%
	Overall:	0.9564	429.3	0.9705	9.867	<0.0001	0.103%

It may be seen that the error increases for the system liquid set, but that is easily explained as the larger doses required by the system liquid results in a higher magnitude of potential error. It is actually striking that the error taken as a percentage of the mean magnitude of the measurement (reported in Table A2 as a percentage relative standard error or RSE) is actually lower. Considering that multiple aspirations are necessary to deliver higher volumes, this decrease in the RSE may be seen as a vindication of the idea that using massive data sets will lead to a degree of self-correction.

In addition to examining these models and their indicators, the residuals are examined by pipette tip, an example of which is shown in Chart A3. Significantly, there is a greater number of outliers for the model at a higher dosing level and this would appear to indicate that the ideal model is not linear in nature, but possibly quadratic. Due to the simple nature of the dispensing apparatus, this is unlikely and it is more likely that a source of error has been introduced that has more of a chance of expressing itself at higher dosages.

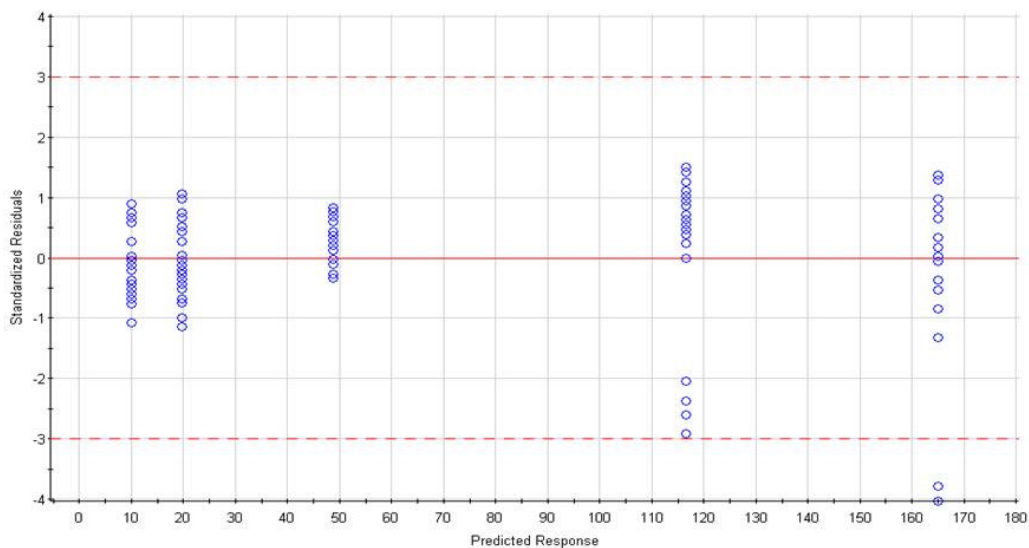


Chart A 3. Residual Error for Pipette Tip#4 Dispensing Neat Substance

One possibility that was considered is that higher dosages require a longer time for the pump to draw the aspirated sample into the pipette tip by virtue of the vacuum produced and the subsequent drive to offset that vacuum via the flow of the neat substance. Put

more simply, when the pipette draws the solution into the tip, enough time must be given to allow equilibration to occur. Withdrawing the tip too soon will result in an error related to the fact that not all of the intended amount was aspirated. Hypothesizing that a slower aspiration rate is needed to ensure that equilibrium is best attained results in the generation of a new set of data, essentially taking the process back to the beginning, but with still significant information in terms of preventing evaporation during the formulation runs and increased care in data collection.

On an even more positive note is the fact that the system liquid does not show the same type of spread from lower levels to higher levels (Chart A4), possibly because the system liquid is dispensed in a manner that does not require aspiration (bolstering the idea posited above). Based on this information, combinations of pipette tips are modeled for the system liquid in an attempt to maximize efficiency (e.g. use as many tips as possible), while minimizing the standard error.

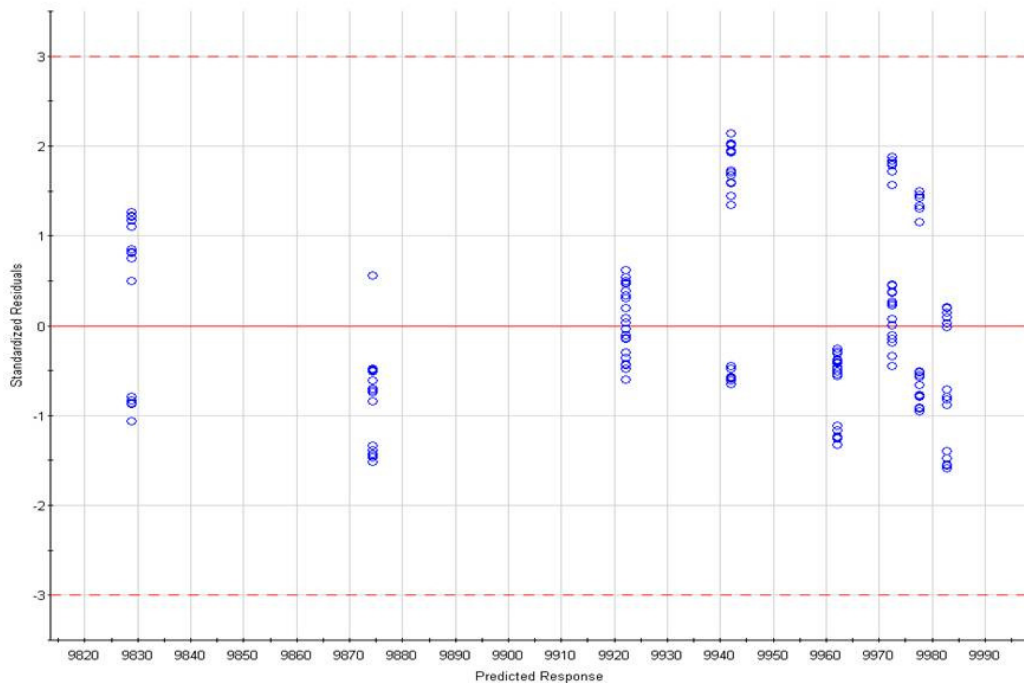


Chart A 4. Residual Error for Pipette Tips Dispensing System Liquid

Various combinations are tried with the existing data, and the results of the combinations tried are shown in Table A3. Utilizing tips 3, 4, 6, and 7 was chosen as a way to

maximize efficiency while keeping the error relatively low, and these tips were utilized in the remainder of the calibration sets. Furthermore, the values of the slope and intercept were used as offset factors to ensure that the Janus formulator provided the closest possible amounts in delivery to what was requested.

Table A3: Models of Combined System Liquid Pipette Delivery Dosages.

Tip #'s	Model: Delivered Dose = Requested*m + b (from $y = mx + b$)					
	Slope (m)	Intercept (b)	Correlation (R^2)	Standard Error (s)	Stat. Significance (p)	Relative Standard Error (RSE)
2,5	0.9663	323.8	0.9965	2.227	<0.0001	0.0232%
1,7,8	0.9799	198.0	0.9866	6.749	<0.0001	0.0703%
3,4,6	0.9588	401.3	0.9744	8.776	<0.0001	0.0914%
3,4,6,7	0.9682	308.9	0.9768	7.785	<0.0001	0.0811%
3,6,7,8	0.9703	291.0	0.9748	9.706	<0.0001	0.1011%
3,4,6,7,8	0.9671	321.5	0.9761	9.064	<0.0001	0.0944%
1,3,4,6,7,8	0.9688	305.2	0.9781	8.310	<0.0001	0.0866%

The next set of data generated thus utilized the 3, 4, 6, and 7 tips for the system liquid and the ensuing data for the system liquid were used to validate whether or not these tips are good choices as the study commences.

A.2 THE SECOND PASS

The next set of data was generated using the preferred system liquid pipettes determined in the first pass and a slower aspiration rate for the neat substance. The overall result of using the lower aspiration rate in terms of data collection is shown in Chart A5 (left). Immediately it was clear that there is greater coherence in the model utilizing all tips. Another point in consideration is the fact that no outliers are removed from the dataset presented. With the first pass the formulator had not been used regularly for a few weeks; it appears that regular usage is helpful in minimizing gross outliers.

As the initial concern was due to increasing error when examining the residuals, that plot was immediately examined as well and is shown in Chart A5 (right). As may be seen, there has been quite a bit of evening out of the residuals across all dosages.

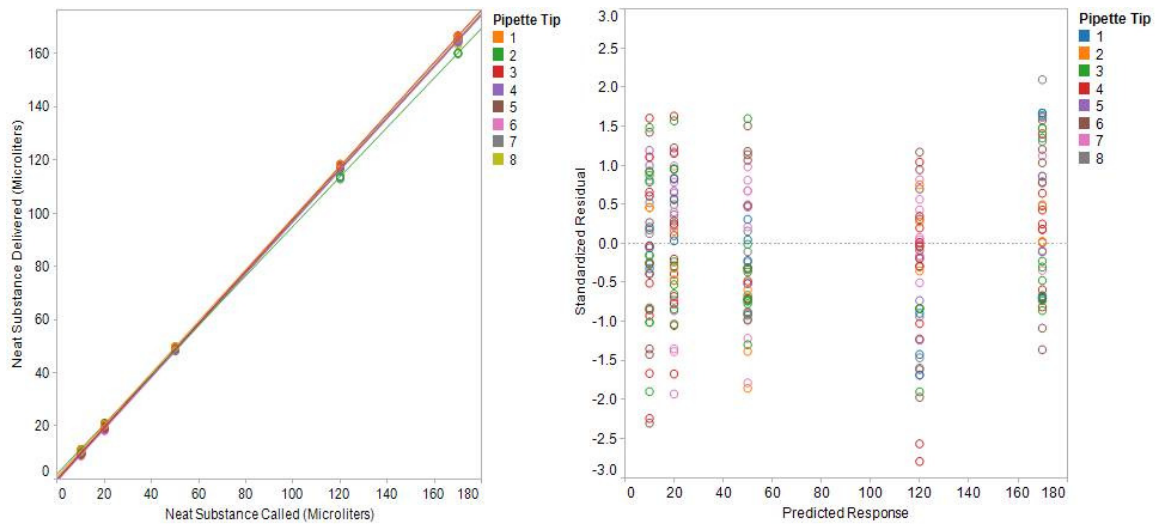


Chart A 5. Dispensing Performance for All Tips with Neat Substance (left) and Residual Error (right)

The next step was to develop estimations of the linear responses to requested neat substance. As before, this step was necessary to ensure the correct correlation between the neat substance requested and the neat substance delivered. Chart A5 showed immediately that Tip #2 clearly diverged from the other tips and so was easily excluded from consideration. The remaining tips show moderate consistency and regressing a line through all data regardless of the tip number (with the exception of Tip #2) produced a model which is not excessively dissimilar from the individual models. The coefficients of all such models are shown in Table A4 as well as measures for the associated variances.

Table A4: Variances in Requested vs. Delivered Dosage by Janus for Second Pass.

Tip #	Model: Delivered Dose = Requested*m + b (from $y = mx + b$)					
	Slope (m)	Intercept (b)	Correlation (R^2)	Standard Error (s)	Stat. Significance (p)	Relative Standard Error (RSE)
1	0.9681	0.4134	0.9999	0.3800	<0.0001	0.317%
3	0.9813	-0.2631	0.9999	0.2814	<0.0001	0.235%
4	0.9760	0.6655	0.9999	1.046	<0.0001	0.872%
5	0.9727	0.09595	0.9999	0.5237	<0.0001	0.436%
6	0.9725	-0.5400	0.9999	0.5344	<0.0001	0.445%
7	0.9810	-0.05275	0.9999	0.4092	<0.0001	0.341%
8	0.9735	1.043	0.9998	0.7599	<0.0001	0.633%
Overall:	0.9748	0.0319	0.9998	0.6122	<0.0001	0.510%

Tip #4 shows the greatest error and Tip #8 shows the lowest correlation, so those two tips were excluded, individually and combined, from the next models and the results are shown in Table A5.

Table A5: Models of Combined Neat Substance Pipette Delivery Dosages.

Tip #'s	Model: Delivered Dose = Requested*m + b (from $y = mx + b$)					
	Slope (m)	Intercept (b)	Correlation (R^2)	Standard Error (s)	Stat. Significance (p)	Relative Standard Error (RSE)
1,3,4,5,6,7,8	0.9748	0.0319	0.9998	0.6122	<0.0001	0.5102%
1,3,5,6,7,8	0.9754	0.09518	0.9998	0.7332	<0.0001	0.6110%
1,3,4,5,6,7	0.9761	-0.06372	0.9998	0.8284	<0.0001	0.6903%
1,3,5,6,7	0.9769	0.03154	0.9999	0.6952	<0.0001	0.5793%
1,3,7	0.9786	0.2424	0.9999	0.5191	<0.0001	0.4326%

Simply using tips 1, 3, and 7, as those were the most consistent performers, did not show a significant reduction in error when compared with the time lost in not utilizing two additional tips. For this reason the tips highlighted above were chosen as the tips to be utilized in neat substance delivery and the offsets provided by the estimated model were programmed into the Janus control program.

As the parameters of the system liquid tips were programmed at the end of the first optimization pass, it was with some anticipation that the data was examined for the system liquid delivery. Chart A6 shows the performance in terms of the liquid delivered vs. the liquid called. Additionally, coefficients for the new models generated from the obtained data are shown in Table A6. Restating these models with each iteration allowed a continual optimization and elimination of variance.

Table A6: Models of the Overall and Individual System Liquid Dosages.

Tip #'s	Model: Delivered Dose = Requested*m + b (from $y = mx + b$)					
	Slope (m)	Intercept (b)	Correlation (R^2)	Standard Error (s)	Stat. Significance (p)	Relative Standard Error (RSE)
3,4,6,7	1.005	-59.95	0.9733	10.35	<0.0001	0.1078%
3	1.004	-48.14	0.9740	10.92	<0.0001	0.1137%
4	1.053	-533.9	0.9865	8.664	<0.0001	0.0902%
6	0.9674	317.8	0.9760	9.774	<0.0001	0.1018%
7	0.9626	368.5	0.9373	11.07	<0.0001	0.1153%

Although the linear relationships developed from regression (and shown as trend lines in the chart) seemed somewhat divergent, the performance of the overall system as compared to the performance of the individual tips was consistent.

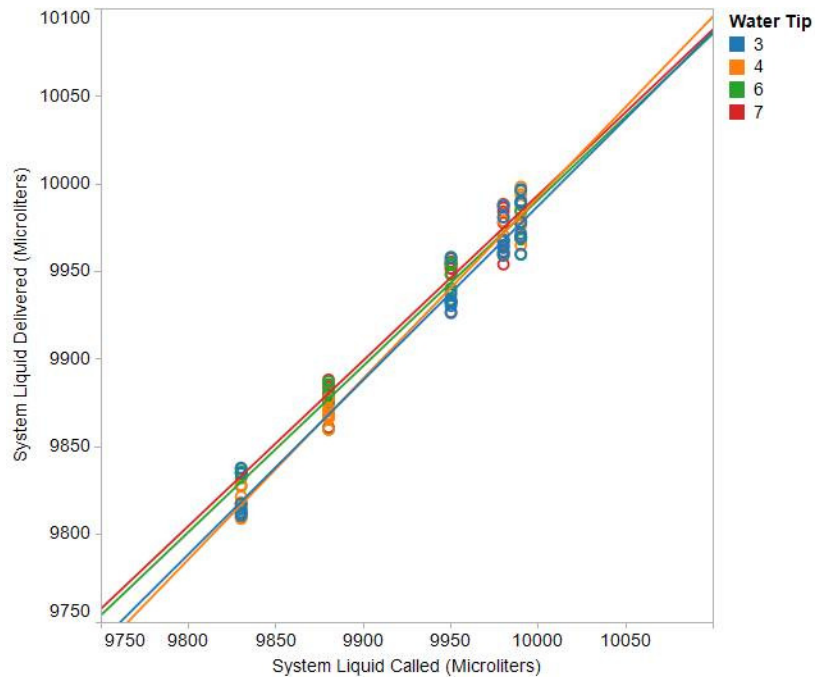


Chart A 6. Dispensing Performance of Chosen Tips with System Liquid

However, examination of residuals showed an anomaly in the range of 9675 μl , as shown in Chart A7. Most residuals are random throughout, but that particular dosage showed a strong shift to a negative error. Taken with the rest of the data, this brought about an overall shift to the positive for the other values. This was a troubling trend and it was hoped that the spectrophotometric method of identifying outliers would be helpful in correcting it.

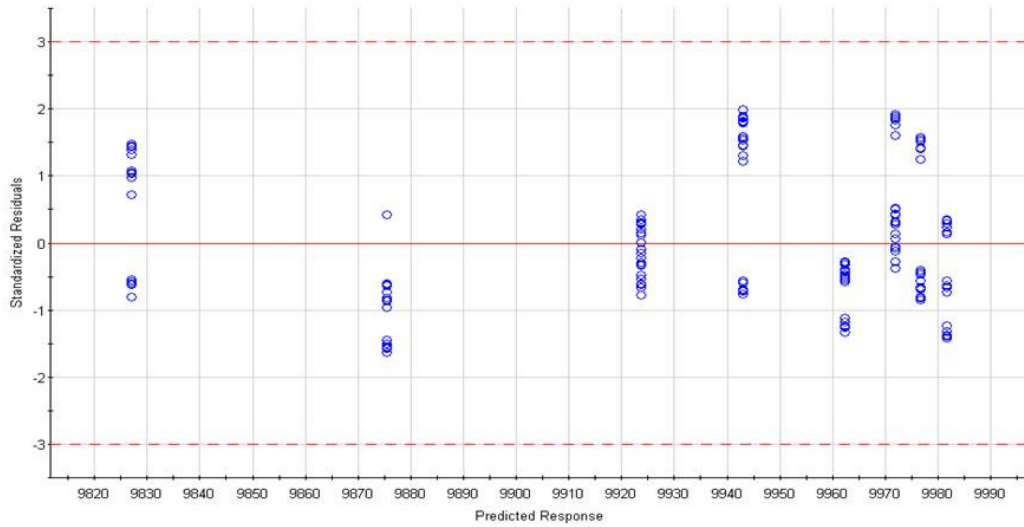


Chart A 7. Outliers Associated with the System Liquid Dispensing Performance of All Selected Tips

A.3 THE THIRD PASS AND VALIDATION

With correlation factors updated and integrating a photometric methodology to eliminate gross outliers (a method fully explained in Appendix B), the Janus formulator was again utilized to make up a series of dilutions by dispensing neat substance and system liquid into receptacles. All data points obtained are shown in Chart A8 (system liquid to the left and neat material to the right), but data points indicated by image analysis as potentially erroneous were then discarded, which resulted in Chart A9.

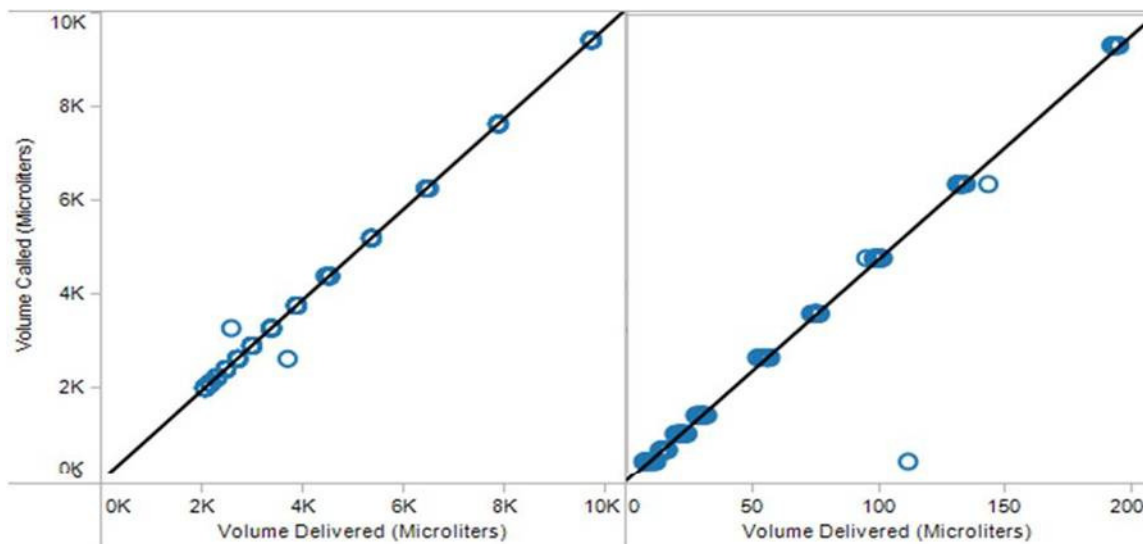


Chart A 8. Raw Data Obtained from Selected Pipettes, System Liquid (left) and Neat Substance (right)

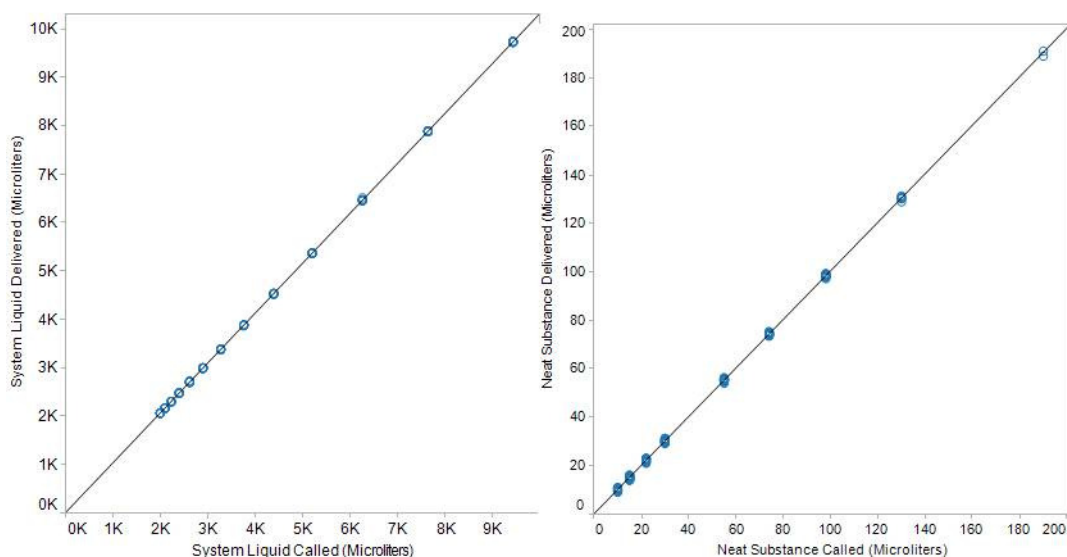


Chart A 9. System Liquid (left) and Neat Substance (right) After Elimination of Outliers

Models were cast on the complete data as well as the “image analysis treated” data and these estimated models are shown along with their variances in Table A7 along with the estimated models developed from the data following the removal of outliers indicated by the image analysis system.

Table A7: Utilized Tips and Associated Model/Offset and Variances

Tip Set	Model: Delivered Dose = Requested*m + b (from $y = mx + b$)				
	Slope (m)	Intercept (b)	Correlation (R^2)	Standard Error (s)	Relative Standard Error (RSE)
Neat Substance (all data)	0.9718	0.5527	0.9790	8.251	6.876%
Neat Substance (outliers removed)	1.002	0.1667	0.9997	0.6342	0.5285%
System Liquid (all data)	0.9686	3.146	0.9979	104.2	1.085%
System Liquid (outliers removed)	1.031	0.2900	0.9999	4.982	0.05190%

By using the image analysis method of identifying suspect points, the correlation was improved and the standard error was significantly reduced. To determine if this treatment of the data maintained statistical significance by preventing a non-random skewing of the data, residuals were plotted for the estimated models shown in Table A7. These residual plots are shown in Charts A10 and A11.

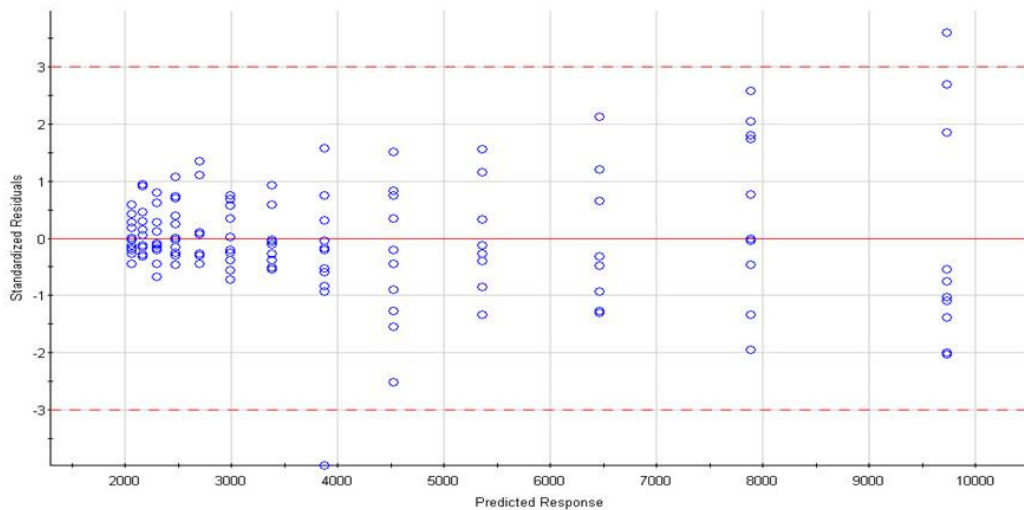


Chart A 10. Residual Error for System Liquid Dispensing

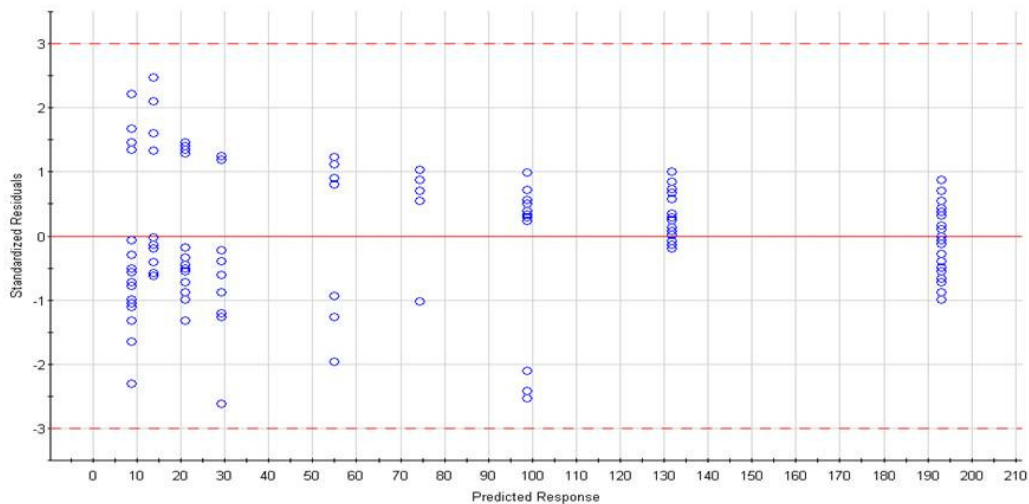


Chart A 11. Residual Error for Neat Substance Dispensing

The offsets employed in instructing the Janus formulator brought the slope and intercept much closer to the ideal values and the tips selected resulted in low variances from the model. Finally, by employing spectrographic image analysis the above tip sets were used for the remainder of the study with a high degree of confidence regarding the concentration of the solutions evaluated.

APPENDIX B

SPECTROPHOTOMETRIC METHOD TO ELIMINATE OUTLIERS

It has been noted that occasional effects such as air bubbles in the delivery line or other unknown environmental effects may lead to gross outliers. These outliers cannot be compensated for via statistical means so a method of detecting them as values far removed from the norm was considered necessary. The simplest idea was simply to use a concentration of visible dye in all surfactant stock solutions (the “neat substance” provided to the Janus formulator) that would be diluted for this study. The hue or intensity of the color would then be directly attributable to concentration of surfactant in accordance with Beer’s Law,

$$A = a_{\lambda}bc$$

in which A is the measured absorbance of light, a_{λ} is the molar absorptivity coefficient, b is the path length, and c is the concentration of the absorbing compound. A simple method of applying this equation is to maintain a constant path length and not to vary the absorbing compound (thus ensuring that a_{λ} does not change). In this way A will linearly vary with c.²⁶

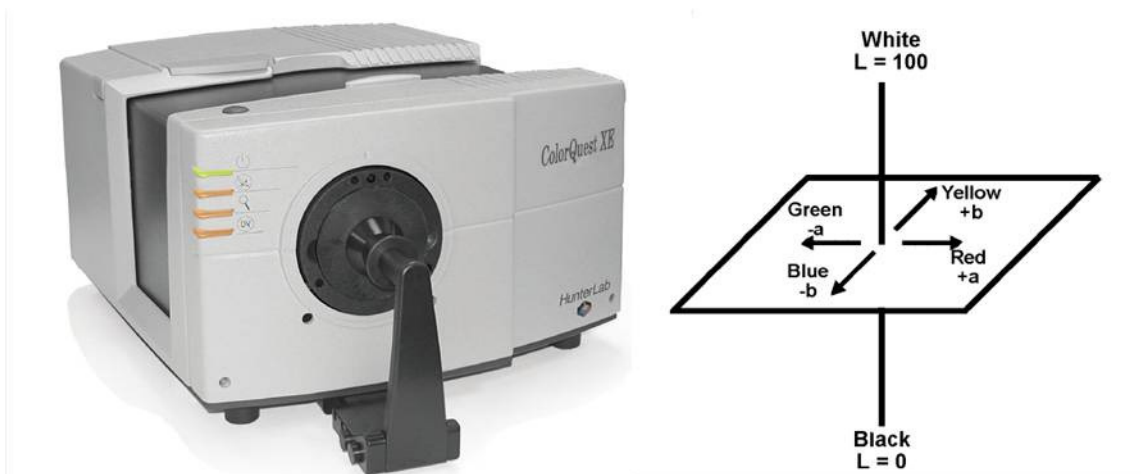
In taking this approach, there were a number of requirements to be met. It was necessary that the dye be visible so that the Image Analysis module of the Janus formulator could be used with no modification to detect the relative color intensity; the dye concentration had to be minute enough to be considered independent of other environmental variances (particularly the inorganic salts or builders intended to test the association of the surfactants); and the dye had to show a correlation with concentration in accordance with Beer’s Law. This last was of some concern because although Beer’s Law has been demonstrated clearly in many ways, the presence of micelles introduces the possibility that solution will cease to be homogenous in absorption. Another way of stating this is that the dye partitioning into the micelle interior might lead to intensifying or fading in the bulk solution in an inverse manner. Due to this physical effect, an improper selection

of dye would cause this method to become meaningless at higher concentrations, causing an overall failure of Beer's Law in this singular case.¹²

If Beers Law does hold, then the spectral data would need to be correlated to the image data collected by the Janus formulator. The Image Analysis module has never actually been used in this manner as the primary use is to determine phase separations and turbidity. The determination of more subtle differences such as hue and intensity, although indicated as possible within the software, is subject to so many environmental variables (voltage fluctuations for the backlight, ambient light, etc.) that there was a lack of certainty that this operation would be possible.

B.1 PROOF OF CONCEPT

The first step was to ensure that concentration could be established by the presence of a visible dye. The Janus formulator was used to prepare a number of samples incorporating the anionic surfactant sodium dodecyl sulfate (SDS) with a dye load of 0.20%. The samples were checked via analytical balance to establish the concentration of dye prior to testing via spectrophotometer. The absorbance was then measured in an inverse manner by utilizing the "transmittance" function of a HunterLAB benchtop spectrophotometer (shown in Picture B1, left) measuring in the CIE L*a*b* color scale which is typically used in analysis of visual hue and intensity.



Picture B1. ColorQuest XE (left) and Graphic Representation of CIE L*a*b* Scale (right)²⁹

The CIE L*a*b* scale is a measurement of light in three dimensions. The first dimension, L, is the “brightness” indicated by either reflectance or absorbance of incidental light. A measure of 100 indicates a complete reflectance or passage of the incidental light which is transmitted between 400 and 700 nanometers. The second two dimensions, a and b, correspond to wavelengths that result in color and are a measure of the balanced reflection or passage of two spectral ranges. In particular, a balances nominally between green and red (ranging from 500 to 700 nanometers) and b balances nominally between blue and yellow (ranging from 400 to 600 nanometers). These second two dimensions are correlated by returning a zero for a “balanced” score (i.e. absorbing equal amounts on both sides of the median of the range). For example, light absorbed heavily in the 400nm wavelength would give a value close to -100 for the b scale, and it was this particular portion of the scale that was utilized. The water soluble dye being used to identify concentration absorbs between 420 and 470 nanometers, thus it would be indicated via the b scale by the spectrophotometer. A pictographic representation of this method of color and intensity “scoring” is shown in Picture B1 (right).²⁹

Samples were prepared utilizing the Janus formulator in conjunction with an analytical balance in the same manner described in Appendix A. A stock solution of SDS and dye was prepared in water as described above and presented to the Janus as neat substance, then diluted by the system liquid. The resulting dilute solutions were measured in the b scale in duplicate. A sample of the raw data from this step is shown in Table B1.

Table B1. Sample of Concentration and Spectral Data

Water Dosed (μl)	Water Call (μl)	Solution (g)	Sol. Dosed (μl)	Sol. Call (μl)	Conc (%)	Dye Conc. (%)	Trans. 1	Trans. 2
9960.2	9990	0.0107	10.7	10	0.04927	0.00994	2.01	2.02
9954.4	9980	0.0202	20.2	20	0.09392	0.01886	3.71	3.71
9954.9	9950	0.0497	49.7	50	0.22761	0.04587	8.59	8.6
9868.5	9880	0.1184	118.4	120	0.54451	0.10956	18.87	18.89
9812.3	9830	0.1668	166.8	170	0.77137	0.15428	25.17	25.19
9969.9	9990	0.0111	11.1	10	0.05179	0.00990	1.96	1.96
9984.4	9980	0.0209	20.9	20	0.09629	0.01929	3.73	3.73
9954.2	9950	0.0498	49.8	50	0.22910	0.04560	8.56	8.55

9871.9	9880	0.114	114	120	0.52519	0.10495	18.25	18.26
9971.9	9990	0.0093	9.3	10	0.04331	0.00865	1.77	1.8
9988.7	9980	0.0192	19.2	20	0.08828	0.01821	3.52	3.55
9948.5	9950	0.0492	49.2	50	0.22866	0.04569	8.52	8.51
9869	9880	0.1177	117.7	120	0.54760	0.10890	18.73	18.71
9810.9	9830	0.1655	165.5	170	0.77041	0.15312	24.94	24.96
9997.1	9990	0.0093	9.3	10	0.04340	0.00835	1.87	1.86
9978.1	9980	0.0182	18.2	20	0.08438	0.01716	3.54	3.52
9938.8	9950	0.0483	48.3	50	0.22259	0.04463	8.48	8.5
9860	9880	0.1171	117.1	120	0.54694	0.10914	18.85	18.86
9838.2	9830	0.1653	165.3	170	0.76065	0.15247	25.07	25.09
9990.4	9990	0.0099	9.9	10	0.04583	0.00873	1.85	1.86
9967.7	9980	0.0191	19.1	20	0.08902	0.01780	3.56	3.56
9940.5	9950	0.0493	49.3	50	0.22920	0.04525	8.49	8.47
9870.6	9880	0.118	118	120	0.54440	0.10932	18.8	18.81
9812.5	9830	0.1667	166.7	170	0.77188	0.15388	25.12	25.13
9969.9	9990	0.0103	10.3	10	0.04786	0.00927	1.91	1.92
9986.7	9980	0.0196	19.6	20	0.09017	0.01799	3.56	3.56
9955.3	9950	0.0487	48.7	50	0.22465	0.04500	8.5	8.5
9866.3	9880	0.1177	117.7	120	0.54092	0.10860	18.84	18.82
9812.9	9830	0.1655	165.5	170	0.76227	0.15163	24.94	24.92

A linear regression analysis was performed via linear least squares with no intercept. The idea was that Beer's Law is linear in nature and the intercept should be zero (no absorbance of blue at no concentration of dye). The results of this regression are shown in Chart B1 and it was immediately clear that the model does not fit well. A clear pattern in the residuals plot (Chart B2) indicated that at least one component was missed in estimating this model.

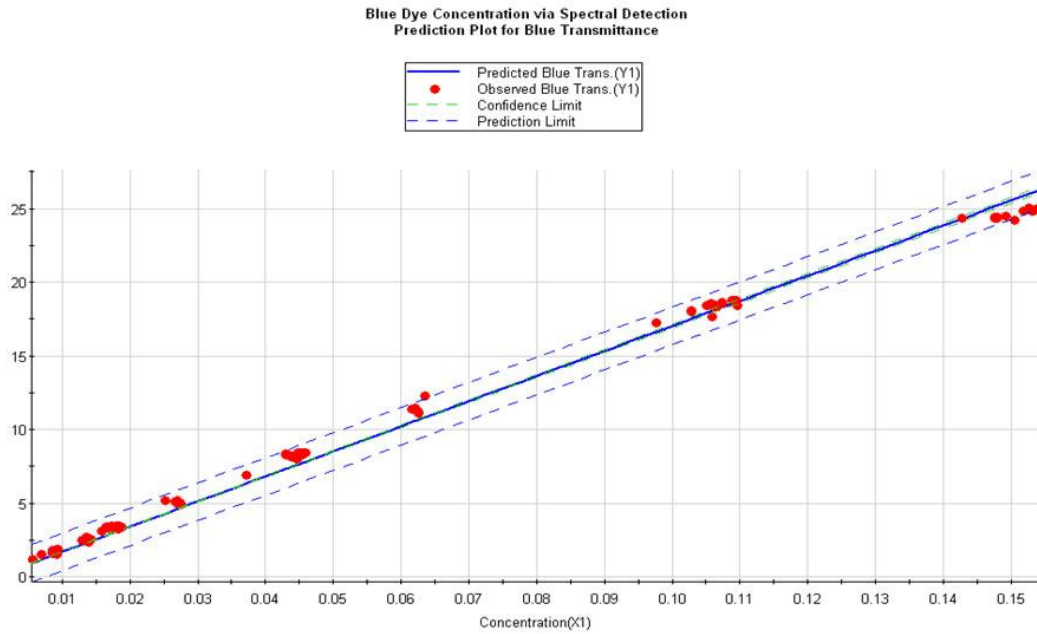


Chart B1. Linear Model Estimate of Blue Transmittance as Related to Concentration.

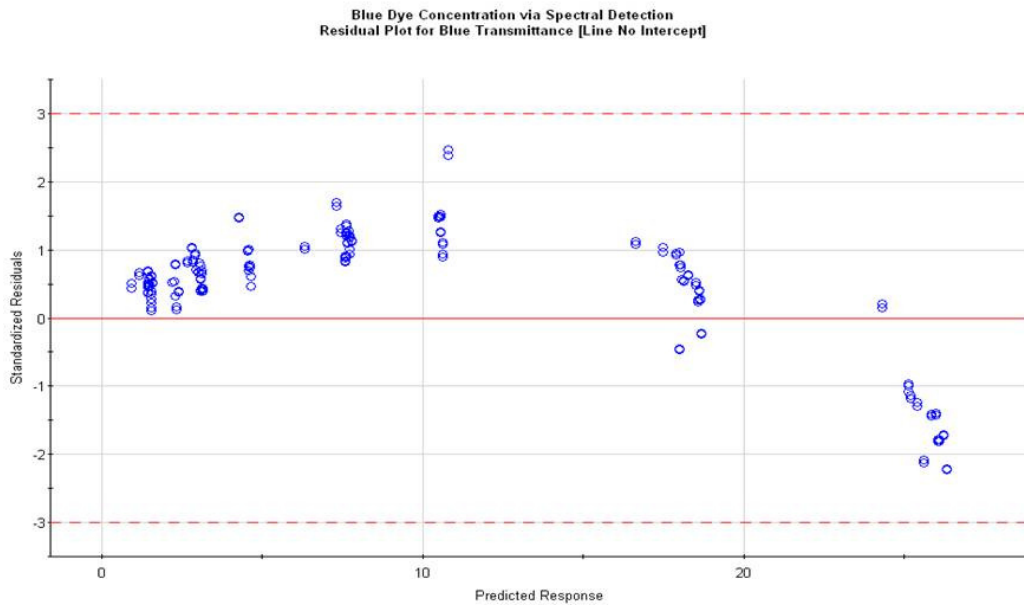


Chart B2. Residuals Plot for Linear Model Estimation of Transmittance vs. Concentration

Changing the model to a quadratic form provided a better estimation of the relationship between the independent variable (concentration) and the dependant variable (transmittance). This is shown in Chart B3 and the residuals bear this out in Chart B4.

Even more importantly, the prediction limit decreased significantly, allowing the use of this curve or relationship to indicate outliers within closer tolerances.

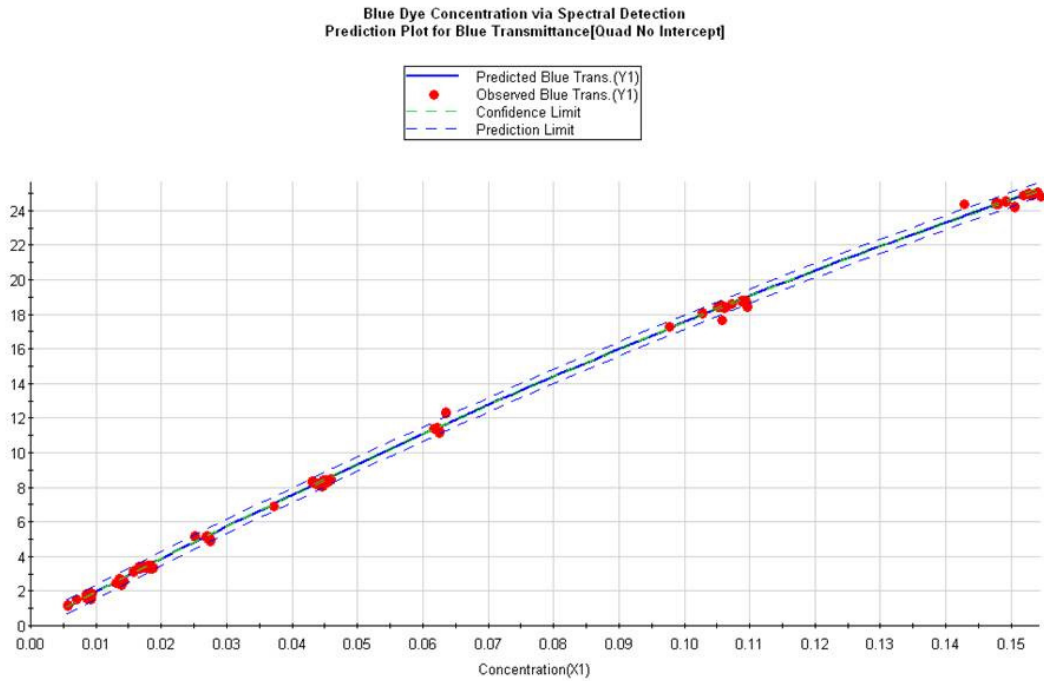


Chart B3. Linear Model Estimate of Blue Transmittance as Related to Concentration

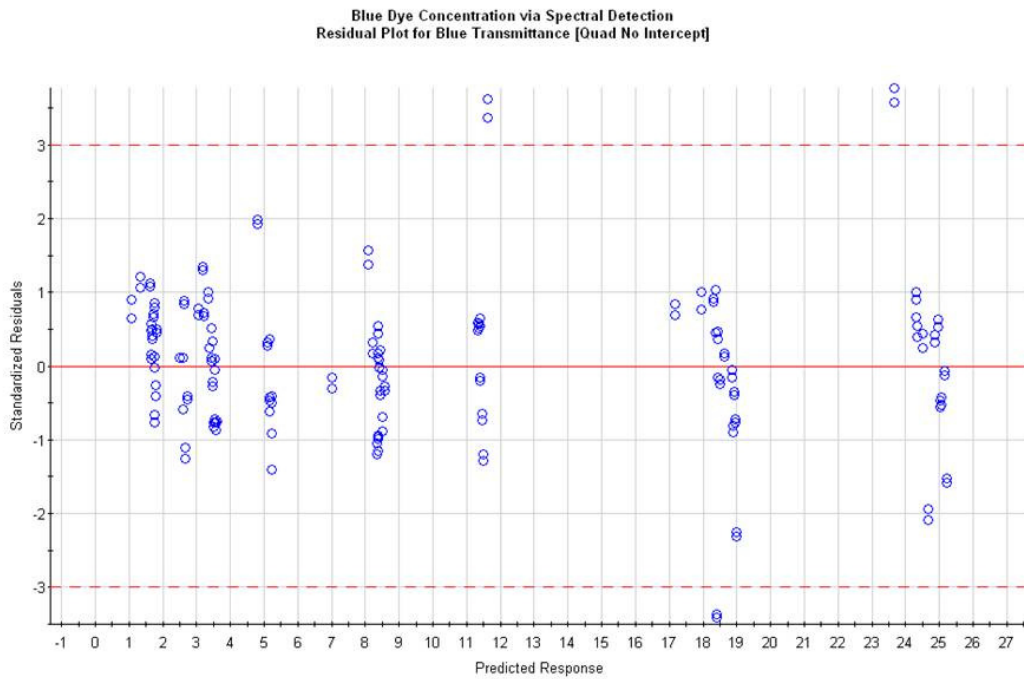


Chart B 4. Plot for Quadratic Model Estimation of Transmittance vs. Concentration

It appears that the idea of micelles interfering with Beers Law has some validity. At lower ranges the concentration of surfactant is well below the critical micelle concentration (CMC), and at the upper limit the surfactant concentration is above the CMC.

Another idea presented during this modeling process was that perhaps the solution itself is responsible for some loss of transmittance because the surfactant may absorb in the range of interest; to determine if this was the case an intercept was calculated through regression and tested against the previous models. The result of this next iteration was very similar to the previous model and there is hardly any change in the Analysis of Variance (ANOVA) on the regressed variables, the R^2 , or the RMSE. Details on these values are shown in Table B2.

Table B2. Statistical Terms and Values Associated with Three Transmittance Regression Models.

Model	ANOVA Results (Term F-Value)			R^2	RMSE
	Intercept	Concentration	Concentration ²		
Linear, No Intercept	--	6.89×10^4	--	0.997	0.646
Quadratic, No Intercept	--	3.34×10^5	7.16×10^4	0.999	0.208
Quadratic w/Intercept	1.32×10^5	2.08×10^4	6.17×10^2	0.999	0.206

Based on the minimal change in variance and a significant lessening of complexity, it was decided to move ahead with the second model (quadratic, no intercept). The equation to calculate expected transmittance of a given concentration was determined as follows:

$$\text{Transmittance} = 198.0 \times \text{Concentration} - 224.8 \times \text{Concentration}^2$$

Solving the quadratic equation for the concentration term and validating allowed the prediction of a concentration of a prepared solution within a given error. A transmittance

outside of the expected error casts enough doubt upon the sample that its data may be discarded with confidence. The equation employed to check the concentration is:

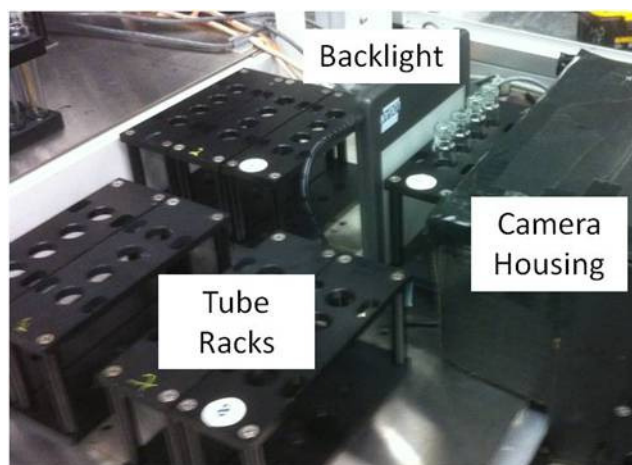
$$\text{Concentration} = 0.4404 - [(39,200 - 899.2 * \text{Trans.})^{0.5} / 449.6]$$

At this point gross outliers would be identified either by predicting the concentration via transmittance or vice versa. Unfortunately, this was quite time consuming for the scope of the study at hand because the volume of solution required for the spectrophotometer is three times the maximum size of a standard sample prepared by the Janus and the cuvettes must be manually prepared and set for a proper reading. The ideal solution had always been to use the Image Analysis module to determine the intensity of blue dye (thus the concentration), because this would allow the instrumentation to essentially “handle” the sample preparation and evaluation in subsequent steps.

This final hurdle in identifying outliers could be surmounted by determining if the Image Analysis module could be precise enough to be correlated with the spectrographic data acquired above. In an attempt to be very flexible in application, some precision in setup was sacrificed when establishing this module, thus the validation of color is anticipated to have more error than a typical spectrophotometric device. For this reason, the image analysis needed be correlated with the transmittance values generated.

B.2 STANDARDIZING THE IMAGE ANALYSIS

The Image Analysis module is shown in Picture B3. The black box to the right is the housing for the camera which acquires an image of four test tubes at one time. The test tubes are illuminated by the backlight which provides a consistent color and intensity of white light. Other test tube racks may be clearly seen, but what is not seen is the robot arm which will move and place the test tubes so that the image acquisition can continue autonomously.



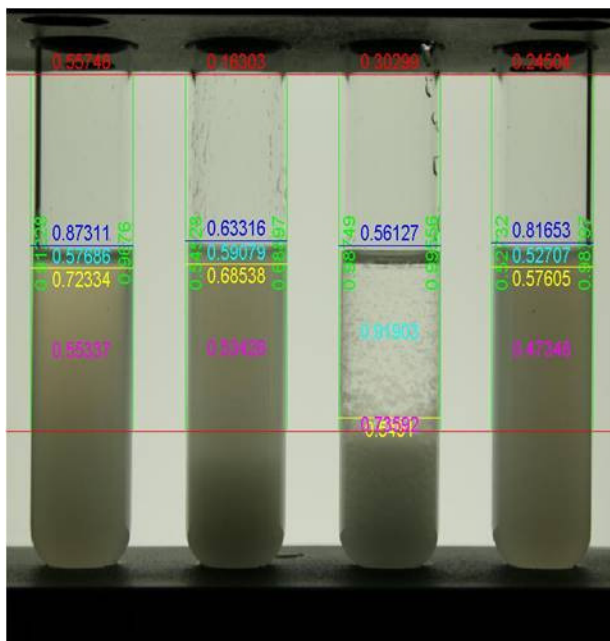
Picture B 2 The Janus Image Analysis Module.

As dilutions are prepared for data acquisition, these dilutions are captured photographically via a Canon EOS Rebel which is held in a fixed bracket by the Janus platform and the image is transmitted to a computer. The camera control software passes the image on to a proprietary Air Products software package for image analysis to determine color, visible light absorbance, and turbidity. Because of the image capture algorithm, a red/green/blue (RGB) color determination is made rather than utilizing the L*a*b* color system supported by the HunterLAB spectrophotometer. The hope was that the blue portion of the spectrum would be closely correlated to the b- value reported by the spectrophotometer. The image capture software also determines an overall absorption and a turbidity score and these were also considered possible indicators of dye presence. An example of some of the raw data collected is shown in Table B2 and a representative image files are shown in Picture B4.

Table B2. Example of Data from the Image Analysis System.

Sample Num	Replicate	Conc.(%)	Module	Position	Height(mm)	Absorb.	Red	Green	Blue	Turb.
1	1	0.012	M01	1	81	0.01897	0.95448	0.96057	0.95671	-1.42792
1	2	0.012	M01	1	81	0.01893	0.95445	0.96060	0.95701	-1.57917
2	1	0.017	M01	2	83	0.01941	0.94366	0.95826	0.96680	0.03804
2	2	0.017	M01	2	83	0.01912	0.94475	0.95857	0.96732	-0.92648
3	1	0.033	M01	3	84	0.02128	0.92518	0.95475	0.97594	6.26334

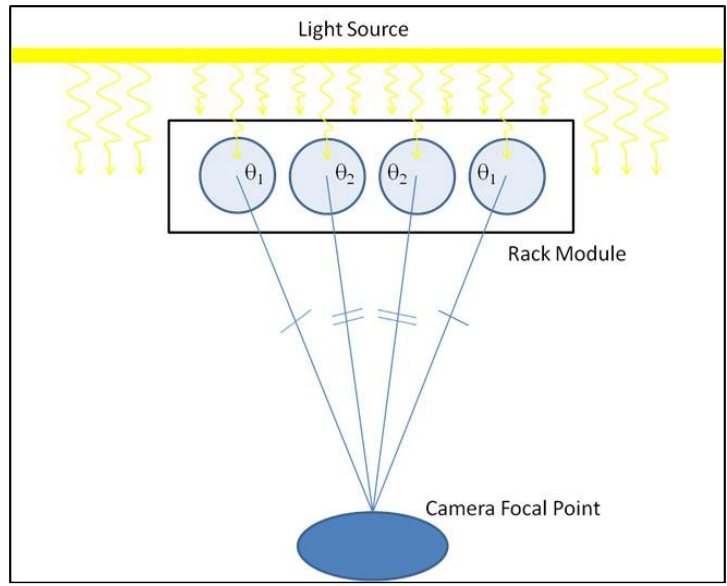
3	2	0.033	M01	3	84	0.0210 5	0.9257 5	0.9553 6	0.9762 5	5.51185
4	1	0.050	M01	4	84	0.0290 1	0.8953 6	0.9419 4	0.9674 4	32.02500
4	2	0.050	M01	4	85	0.0286 2	0.8969 7	0.9426 6	0.9676 7	30.73348
5	1	0.117	M02	1	96	0.0103 1	0.9697 9	0.9804 2	0.9793 6	-30.29275
5	2	0.117	M02	1	86	0.0198 0	0.9492 5	0.9600 1	0.9570 0	1.33596
6	1	0.167	M02	2	100	0.0391 3	0.7946 8	0.9204 2	1.0132 0	65.77973
6	2	0.167	M02	2	91	0.0483 8	0.7741 1	0.9025 2	0.9934 9	96.60551
7	1	0.250	M02	3	102	0.0307 4	0.8335 0	0.9380 9	1.0145 0	37.81563
7	2	0.250	M02	3	91	0.0397 7	0.8139 7	0.9213 8	0.9932 0	67.90031
8	1	0.317	M02	4	101	0.0381 8	0.8170 0	0.9242 2	0.9973 0	62.60409
8	2	0.317	M02	4	90	0.0475 7	0.7947 6	0.9069 0	0.9775 9	93.90246
9	1	0.012	M03	1	86	0.0219 9	0.9372 5	0.9569 5	0.9575 7	8.61792
9	2	0.012	M03	1	86	0.0220 6	0.9366 1	0.9571 1	0.9575 2	8.88189
10	1	0.017	M03	2	88	0.0218 3	0.9273 8	0.9534 6	0.9715 5	8.11134
10	2	0.017	M03	2	88	0.0216 6	0.9277 0	0.9539 1	0.9719 2	7.53239
11	1	0.033	M03	3	87	0.0221 9	0.9154 0	0.9529 7	0.9810 4	9.30773
11	2	0.033	M03	3	87	0.0228 0	0.9143 6	0.9516 7	0.9793 9	11.34522
12	1	0.050	M03	4	88	0.0195 6	0.9489 2	0.9603 0	0.9586 0	0.54468
12	2	0.050	M03	4	88	0.0192 3	0.9494 9	0.9609 7	0.9595 8	-0.57630
13	1	0.117	M04	1	84	0.0229 9	0.9320 7	0.9553 0	0.9577 2	11.97657
13	2	0.117	M04	1	84	0.0230 9	0.9316 9	0.9548 1	0.9579 7	12.28920
14	1	0.167	M04	2	89	0.0396 4	0.8214 6	0.9221 7	0.9870 1	67.48080
14	2	0.167	M04	2	89	0.0394 1	0.8216 7	0.9226 4	0.9877 7	66.69554
15	1	0.250	M04	3	89	0.0394 3	0.8160 3	0.9226 2	0.9923 5	66.75478
15	2	0.250	M04	3	88	0.0391 8	0.8167 8	0.9228 7	0.9929 1	65.94582
16	1	0.317	M04	4	87	0.0556 1	0.7480 3	0.8882 8	0.9867 2	120.7006 9
16	2	0.317	M04	4	88	0.0558 3	0.7473 5	0.8882 0	0.9861 2	121.4312 3



Picture B 3. Treated Photo from Image Analysis

The rack holding the test tubes is referred to as a “module” and each module may hold 4 test tubes. Consideration of the geometry of the optical path (Picture B4) immediately identifies a potential problem with correlation. Tubes at position 1 and 4 and tubes at position 2 and 3 form two subsets due to the variation of distance and angle of scatter in relation to the camera lens. The altered distance (or pathlength, variable b in the Beer’s Law equation) will produce two different intensities of light (1 and 4 vs. 2 and 3) and the altered scatter angle will produce two different groupings of wavelengths due to elastic (Rayleigh) and inelastic (Raman) scattering and how the angle of scatter impacts the potential shift.²⁶ It was possible (even likely) that these two effects would have no impact within the range of experimental error, but the effect had to be ruled out before making that assertion.

Measurements were taken within subsets of rack position and optical range (red, blue, or green). The resulting spread is shown in Chart B4 and it is clear that an immediate correlation was not found. In the red optical range it appears that more differentiation is seen among concentrations than in the other ranges so data set formed from observations in the red range was examined more closely. The correlation values for each rack position are shown in Table B3.



Picture B 4. Illustration of Module Imaging Variance for Tubes

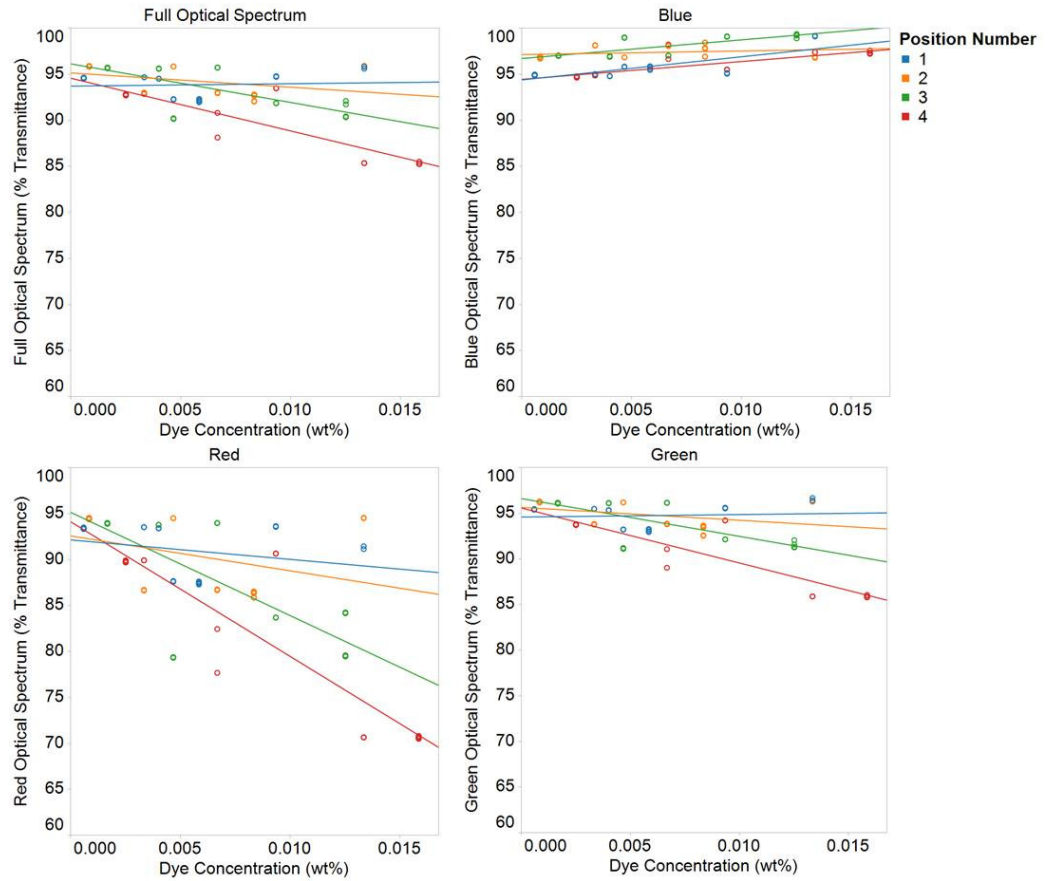


Chart B 5. Transmission of Color Spectra as Determined by Image Analysis

Table B3. Model Correlation of Dye Concentration in the Red Optical Spectrum with the Image Analysis Module Open to the Ambient Light

Rack Position	Model: % Red Transmittance = Concentration*m + b (from $y = mx + b$)				
	Slope (m)	Intercept (b)	Correlation (R^2)	RMSE	Significance (p)
1	-212.0	92.13	0.0806	2.800	0.2003
2	-379.2	92.56	0.1390	3.950	0.1056
3	-1124	95.13	0.5810	4.448	<0.0001
4	-1465	94.11	0.8263	4.026	<0.0001

Needless to say, the concern over two different path lengths was misplaced; all four positions within the rack have a correlation different from the rest. It is also clear that Position 4 has the single best model correlation and some thought was expended upon why that might be. Eventually a theory was formed.

A glance back to Picture B2 shows how the Image Analysis module is typically open to the surroundings, and considering how and why the method is employed, it has always been suitable to do so. Phase separation provides a hard interface that a canny operation (the photo detection of a change in surface is referred to as “canny”) can generally find. Turbidity is the detection of opacity within a substance. In both cases, the exclusion of light is the primary focus, but in the case of the optical recognition of color, light is integral, which is why it was only with this new method that a realization developed that incidental light from the surrounding lab may have an impact.

The solution was simply to enclose the Image Analysis module. Another set of concentrations were prepared, analyzed, and plotted. The resulting plot is shown in Chart B4. Not only did the correlation markedly improve, but the positions correlated with each other and a linear relationship appeared to be a good fit. In retrospect the precision that was lost in moving from a spectrophotometer to photometric may be responsible for making the model simpler yet still useful.

Table B4. Model Correlation of Dye Concentration in the Red Optical Spectrum with the Image Analysis Module Enclosed

Rack Position	Model: % Red Transmittance = Concentration*m + b (from $y = mx + b$)				
	Slope (m)	Intercept (b)	Correlation (R^2)	RMSE	Significance (p)
All Positions	-1479	95.33	0.9713	1.390	<0.0001
Position 1&4	-1602	95.66	0.9899	0.9142	<0.0001
Position 2&3	-1345	94.90	0.9755	1.142	<0.0001

Another interesting point is that now the grouping of positions 1 & 4 and 2 &3 may be seen to have an impact. Close examination of Chart B6 makes this clear, although it may also be seen from the correlations presented in Table B4; by grouping those two sets, the precision of the model improves in both cases. For this reason as the sample preparation moved forward, the keep/discard decision was made based on the score of the color as well as the position in the rack. A more rigorous regression was carried out to produce the coefficients shown in Table B5.

Table B5. Calibration Model Used in Determining if a Sample was Correct

Rack Position	Model: Concentration = % Red Transmittance *m + b (from $y = mx + b$)				
	Slope (m)	Intercept (b)	Correlation (R^2)	RMSE	Significance (p)
Position 1&4	-0.0606	0.0579	0.9606	0.011	<0.0001
Position 2&3	-0.0681	0.0652	0.9696	0.001	<0.0001

Inverting Concentration from independent to dependant, two new models were cast so that decision points were assessed with each prepared. If the difference between the intended concentration (as programmed into the Janus) and the analyzed concentration (taken from the Image Analysis calibration model) was greater than 3 times the RMSE of the model, the sample was discarded as being potentially flawed.

APPENDIX REFERENCES

²⁸ PerkinElmer. JANUS Automated Workstation. 2011.
<http://www.perkinelmer.com/Catalog/Category/ID/JANUS>.

²⁹ HunterLab. ColorQuest XE. 2010. <http://www.hunterlab.com/Instruments/Bench/ColorQuestXE>.

VITA

Eric Ross Theiner (“Rick”) was born at Andrews Air Force Base in Maryland. Having spent his formative years in Memphis, TN, he attended Christian Brothers University in the same city and earned a Bachelor of Science degree in Chemical Engineering in May, 1990. Following this achievement he entered industry and worked primarily in research and product development of cleaning products used in industrial and institutional settings.

In 2004 Rick went to work for Tomah Products in Milton, WI to focus on surfactant development, again primarily in cleaning applications, but also in other market segments. Following the acquisition of Tomah Products by Air Products and Chemicals, Inc., Rick relocated to Allentown, PA and entered the Graduate School at Lehigh University in Bethlehem, PA in the fall of 2008. During this time he maintained his full-time position as Principle Applications Chemist and continues to contribute to the success of the Performance Materials Division in that way. As of this writing he remains in Allentown with his wife and two sons.

Permanent Address: 1322 Cobbler Lane
 Allentown, PA 18104